Photoinduced Intramolecular Charge Transfer in a Series of Differently Twisted Donor−Acceptor Biphenyls As Revealed by Fluorescence

Michael Maus[§] and Wolfgang Rettig*

W. Nernst-Institut für Physikalische und Theoretische Chemie, Humboldt-Universität zu Berlin, Bunsenstrasse 1, D-10117 Berlin, Germany

Dominique Bonafoux and René Lapouyade*

Laboratoire des Sciences Moléculaires, Institut de Chimie la Matière Condensée de Bordeaux, Avenue du Dr A. Schweitzer, F-33608 Pessac Cedex, France

Received: February 10, 1999

This photophysical study addresses the general question of how electron transfer in bichromophoric molecules influences the conformational relaxation, which can be toward either more or less π-conjugation. The effects of photoinduced intramolecular charge transfer on the electronic and molecular properties of a series of differently twisted 4-*N*,*N*-dimethylamino-4′-cyanobiphenyls are investigated by steady-state and time-resolved fluorescence. The dipole moments, radiative rates, and torsional relaxations in the excited state are analyzed by comparison with the absorption spectra and interannular twist angle (φ)-dependent CNDO/S calculations. Independent of the twist angle φ and solvent polarity, the first excited singlet state of these donor−acceptor (D−A) biphenyls (**I**−**III**) is an emissive intramolecular ^{1}CT state of the ^1L_a-type transferring charge from the dimethylaminobenzene (D) to the cyanobenzene (A) subunit. Similar to the planar restricted D−A fluorene **I**, the flexible D−A biphenyl **II** shows only a weak dependence of the fluorescence radiative rate constants k_f (0.4−0.6 ns^{-1}) on the solvent polarity, consistent with a planarization in the excited state of **II**. In contrast, the strongly pretwisted biphenyl **III** behaves similarly to **I** and **II** only in nonpolar solvents ($\langle k_f \rangle = 0.3$ ns^{-1}, indicating partial excited-state relaxation toward planarity), whereas with increasing polarity the mean radiative rate $\langle k_f \rangle$ decreases down to 0.03 ns^{-1}. A fast equilibrium between a more planar and a more twisted rotamer distribution in the ^{1}CT state of **III** explains the appearance for **III** of additional photophysical effects such as (a) strong decrease of the radiative rates with increasing polarity, (b) two long (>200 ps) fluorescence lifetimes with precursor−successor relation, and (c) excited-state quenching by protic solvents.

1. Introduction

One of the main challenges of applied research is the use of solar energy. The primary step to convert solar energy into chemical or electrical potential is photoinduced energy or charge transfer. To optimize the whole photoconversion process, the mechanisms of the primary steps, e.g., forward and back charge transfer, have to be understood. For this long-term goal, molecular model systems are needed that allow a convincing and clear analysis of the electronic and geometrical structure before and after the primary step of charge transfer. In the field of intramolecular charge transfer between strongly coupled organic donor and acceptor fragments (fast forward charge transfer) especially, the essential conformational dynamics are usually not known. As an example, the photoinduced charge transfer in dimethylaminobenzonitrile (DMABN), one of the simplest donor−acceptor molecules, has been under controversial discussion for more than 20 years.[1−5] There is no agreement whether the necessary conformational change is toward more or less π-conjugation. In biaryls and especially donor−acceptor biphenyls, donor (D) and acceptor (A) units are more clearly defined and they should therefore serve as less problematic model compounds for the study of photoinduced charge transfer.

In unsubstituted biphenyl (BP), charge-transfer interactions can be neglected and the first excited singlet state (S_1) is a short-axis polarized ^1L_b-type state with low radiative rates ($k_f = 0.01$ ns^{-1}).[6−9] In numerous publications[8,10−13] about the conformational structure of BP in solution, it has been worked out that in the ground state (S_0) the interannular twist angle φ amounts to between 15° and 40°, whereas in S_1 the planar geometry is preferred. The related 4-vinylbiphenyl (VBP) and *p*-terphenyl (TP) have the same tendency in S_1 to relax toward planarity,[8,13] but because of a state inversion in comparison to BP, a long-axis polarized state of the ^1L_a-type associated with a much faster radiative transition (VBP: $k_f = 0.24$ ns^{-1}; TP: $k_f = 0.98$ ns^{-1}) becomes the lowest lying excited-state S_1.[8] Now it is of interest to elucidate what consequences arise when charge-transfer interactions are introduced. Several previous studies on D−A biphenyls are known,[14−25] but most of them show nontrivial photophysics strongly changing with solvent or solvent polarity, which complicates the assignment to well-defined electronic and conformational structures. The undesirable side-effects encountered in known D−A biphenyls containing considerable charge-transfer character in the first excited state can be divided into three classes: (1) electronic nature of mixed character, between that of biphenyl (^1L_b-type) and 4-vinylbiphenyl (^1L_a-type), (2) strong and solvent-polarity-dependent nonradiative channels due

[§] Present address: Laboratory for Molecular Dynamics and Spectroscopy, Department of Chemistry, K. U. Leuven, Celestijnenlaan 200 F, B-3001 Leuven-Heverlee, Belgium.

10.1021/jp9905023 CCC: $18.00
Published on Web 04/20/1999

SCHEME 1. Molecular Structures of the Donor−Acceptor Biphenyls Investigated (I−III) and Their Corresponding Equilibrium Ground State Twist Angles φ_{gas} As Obtained by AM1 Calculations

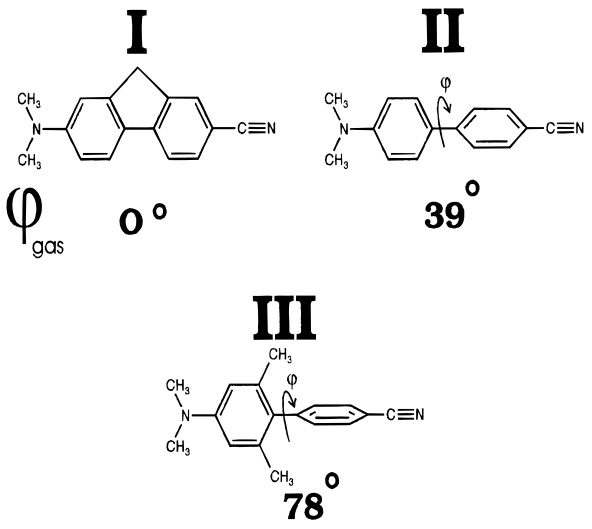

to intramolecular processes, and (3) strong nonradiative channels due to specific solvent interactions.

Let us briefly cite some examples for these three categories.

Category (1). Para-amino substituted biphenyls such as 4-diethylaminobiphenyl (EBA) show radiative rates that are only slightly larger ($k_f = 0.02$ ns^{-1}) in alkanes than that for BP, whereas in polar solvents such as acetonitrile ($k_f = 0.05$ ns^{-1}) they are between the rates of BP and VBP.[22] This indicates that the excited-state electronic structure changes with increasing polarity from more ^1L_b-type to more ^1L_a-type.

Category (2). 4-(Dimethylamino)-4′-nitro-biphenyl (DNB), which is the first well-studied biphenyl with donor and acceptor substituents, is highly nonradiative in nonpolar solvents as a result of the nitro group.[20] Similar effects have been observed for 4-(dimethylamino)-4′-formyl-biphenyl (FDBP) in which the nitro group is replaced by an aldehyde group. Here, the nonradiative channel was found to be polarity-dependent.[18]

Category (3). FDBP and a D−A biphenyl with a pyrimidine ring as the acceptor phenyl unit undergo specific interactions with alcohols.[16,18] The hydrogen bonding effects manifest themselves by increased nonradiative rates, shifted absorption and fluorescence maxima in ethanol as compared to equipolar but aprotic acetonitrile.

One purpose of this paper is to show that the newly synthesized series of differently twisted donor−acceptor biphenyls in Scheme 1 do not exhibit the complications discussed above. Although the D−A biphenyl **II** has already been investigated by F. Lahmani et al.,[14] the additional photophysical study of model compounds **I** and **III** in relation to the interannular twist angle φ should allow us to handle the problems discussed above and to draw the desired conclusions about electronic and molecular structure.

In a previous quantum chemical study,[26] the electronic structure of the D−A biphenyls **I**−**III** is interpreted in terms of a composite-molecule model [27,28] with dimethylaniline as the donor fragment (D) and benzonitrile as the acceptor fragment (A). It was pointed out that in contrast to BP a charge transfer state (^{1}CT) becomes very low lying close to the ^1L_b state responsible for the fluorescence in BP. The quantitative configuration interaction (CI) analysis revealed that the ^{1}CT state in the gas phase consists of about 90% HOMO−LUMO

SCHEME 2. HOMO−LUMO Configurations Constituting the ^{1}CT State of I−III by ∼90%[a]

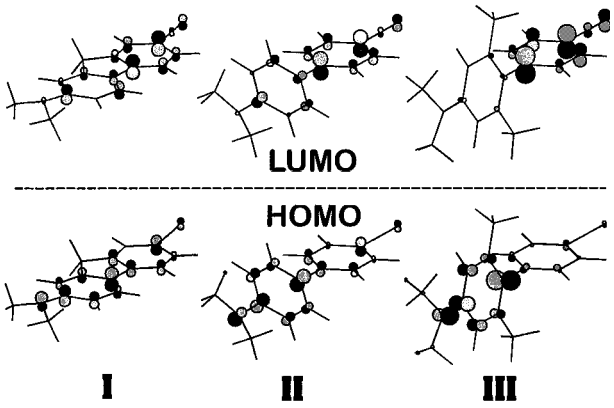

[a] Orbital localization, which is induced with increasing twist angle φ, enlarges the permanent dipole moment and decreases the transition dipole moment.

configuration (Scheme 2), which is a mixture of ^1L_a and electron transfer (^{1}ET)[29] character.[26] The (net) ^{1}ET character is due to the electron promotion from the HOMO(D) to the LUMO(A) orbitals and increases with the twist angle φ.[26,30]

From time-resolved transient absorption experiments, we know that the charge-transfer process in the excited state occurs in the very first picoseconds.[31] However, from the quantum chemical and transient absorption studies alone it could not be derived whether the photoinduced solvent and conformational relaxations diminish the influence of an ^1L_b state on S_1 completely.

Here, we investigate the fluorescence at room temperature and compare it to the absorption behavior to gain further insight into the photophysics and conformational behavior of **I**−**III** following the photoinduced charge transfer.

2. Experimental Section

2.1 Synthesis of the Compounds. 2-*N*,*N*-Dimethylamino-7-cyanofluorene (**I**) and 4-*N*,*N*-dimethylamino-4′-cyanobiphenyl (**II**) were prepared from the commercial aminobromo derivatives in two steps: (1) reductive methylation of the amino group with sodium cyanoborohydride and formaldehyde[32] and (2) subsequent substitution of the bromo substituent by a cyano group.[33] 4-*N*,*N*-Dimethylamino-2,6-dimethyl-4′-cyanobiphenyl (**III**) has been obtained in three steps: (1a) bromination of 1-*N*,*N*-dimethylamino-3,5-dimethylbenzene with 2,4,4,6-tetrabromo-1-cyclohexadienone,[34] (1b) monocyanation of 1,4-dibromobenzene,[35] and (3) a cross-coupling reaction[36] of the organozinc derivative of 1-*N*,*N*-dimethylamino-3,5-dimethyl-4-bromo benzene with 4-bromobenzonitrile, catalyzed by Pd^0.

Data for I: mp 226 °C; MS *m*/*z* (%, fragment): 234 (100, $M^{+\bullet}$), 190 (34), 117 (11). ^{1}H NMR ($CDCl_3$): δ 2.93 (s, 6H, $N(CH_3)_2$), 3.63 (s, 2H, CH_2), 6.63 (s + d, 2H), 7.33 (m, 4H).

Data for II: mp 217 °C; MS *m*/*z* (%, fragment): 222 (100, $M^{+\bullet}$), 206 (13), 111 (11). ^{1}H NMR ($CDCl_3$): δ 3.05 (s, 6H, $N(CH_3)_2$), 6.88 (s, 2H), 7.59 (d, 2H), 7.7 (m, 4H).

Data for III: mp 132 °C; MS *m*/*z* (%, fragment): 250 (100, $M^{+\bullet}$), 234 (16), 190 (12). ^{1}H NMR($CDCl_3$): δ 2 (s, 6H, CH_3), 2.9 (s, 6H, $N(CH_3)_2$), 6.5 (s, 2H, ortho of $N(CH_3)_2$), 7.4 (m, 4H).

2.2. Solvents. The solvents purchased from MERCK were of spectroscopic grade except triacetine (distilled twice) and isopentane (HPLC grade). The absorption and fluorescence

TABLE 1: Excited-State Dipole Moments with ($\mu_e(F_2)$) and without ($\mu_e(L)$) Contribution of the Solute Polarizability using Eqs 6 and 7[a]

I		II		III	
$\mu_e(F_2)$	$\mu_e(L)$	$\mu_e(F_2)$	$\mu_e(L)$	$\mu_e(F_2)$	$\mu_e(L)$
21.3 D	15.0 D	22.0 D	15.5 D	27.2 D	18.6 D

[a] Using the spectral data of Table 2 (except BCl), all correlation coefficients r obtained are better than 0.99.

TABLE 2: Spectroscopic Data of I−III at 298 K in Dependence of the Solvent and Dielectric Constant: Absorption and Fluorescence Transition Energy Maxima ν_a^{max} and ν_f^{max}, Stokes Shifts $\Delta\nu_{St}$, and Band Half-Widths HW (all in 10^3 cm^{-1})

solvent[a]	ϵ_r[c]	ν_a^{max}	ν_f^{max}	$\Delta\nu_{St}$	HW_a	HW_f
			I			
HEX[b]	1.9	27.93	26.89	1.0	3.5	2.5
IpM[b]	1.9	27.93	26.93	1.0	3.6	2.5
MIp[b]	2.0	27.78	26.84	0.9	3.4	2.3
BOB	3.1	27.93	25.97	2.0	4.0	2.5
EOE	4.2	28.09	25.13	3.0	3.8	2.8
TAC	7.1	28.65	23.58	5.1	4.0	3.0
BCl	7.2	27.78	24.81	3.0	3.7	2.5
BCN	24.1				3.8	
EtOH	24.5	27.78	22.47	5.3	4.2	3.2
ACN	36.2	27.86	22.47	5.4	4.0	3.0
DMF	37.0					
MMF	182.4	27.47	21.93	5.5	4.1	3.1
$\Delta_{HEX-ACN}$		0.08	4.42	−4.3	−0.5	−0.5
			II			
HEX[b]	1.9	29.85	26.64	3.2	4.3	2.7
IpM[b]	1.9	29.94	26.73	3.2		2.7
MIp[b]	2.0	29.76	26.66	3.1	4.4	2.5
BOB	3.1	29.50	25.64	3.9	4.5	2.6
EOE	4.2	29.41	24.51	4.9	4.6	3.0
TAC	7.1	29.50	23.04	6.5	5.2	3.0
BCl	7.2	29.07	24.81	4.6	4.8	2.5
BCN	24.1	28.90			4.9	
EtOH	24.5	28.99	21.93	7.1	4.8	3.4
ACN	36.2	29.07	21.79	7.3	5.1	3.1
DMF	37.0					
MMF	182.4	28.49	21.28	7.2	5.5	3.3
$\Delta_{HEX-ACN}$		0.78	4.85	−4.1	−0.8	−0.4
			III			
HEX[b]	1.9	32.05	26.97	5.1	5.0	3.6
IpM[b]	1.9	31.95	26.95	5.0	5.2	3.5
MIp[b]	2.0	31.75	26.84	4.9	5.2	3.4
BOB	3.1	31.75	25.00	6.7	5.1	3.5
EOE	4.2	32.05	23.42	8.6	5.4	4.0
TAC	7.1	32.15	20.66	11.5	5.6	4.4
BCl	7.2	31.75	23.04	8.7	5.9	3.7
BCN	24.1	31.85	19.69	12.2	6.0	4.4
EtOH	24.5	32.05	18.69	13.4	6.2	5.1
ACN	36.2	31.95	18.73	13.2	5.9	4.6
DMF	37.0	31.75	18.66	13.1		4.8
MMF	182.4	31.65	17.73	13.9	5.6	5.4
$\Delta_{HEX-ACN}$		0.10	8.24	−8.1	−0.9	−1.0

[a] The solvent abbreviations are explained in the experimental section. [b] The maxima of the emission spectra with vibrational structure (in HEX, IpM, and MIp) are derived from log-normal fits. [c] Static dielectric constants ϵ_r and refractive indices n (not shown) are taken from ref 53.

spectra of all solvents were checked for impurities and have been subtracted from the sample spectra to ensure they are free from background effects, e.g., Raman and Rayleigh peaks. The abbreviations for the 12 solvents used in the text and also collected in Table 2 are as follows: *n*-hexane (HEX), diethyl ether (EOE), acetonitrile (ACN), ethanol (EtOH), 4:1 mixture of isopentane/methylcyclohexane (IpM), 3:1 mixture of methylcyclohexane/isopentane (MIp), di-*n*-butyl ether (BOB), triacetine (TAC), *n*-butyl chloride (BCl), *n*-butyronitrile (BCN), *N*,*N*-dimethylformamide (DMF), and *N*-monomethylformamide (MMF).

2.3. Steady-State Absorption. The absorption spectra presented were recorded on a ATI UNICAM UV4 UV−vis spectrophotometer, and the decadic molar extinction coefficients ϵ_{max} were repeatedly determined.

2.4. Steady-State Fluorescence. All steady-state fluorescence spectra were obtained on a Aminco Bowman 2 fluorimeter using a 150 W Xe lamp, 2 nm excitation and emission band-pass, and a photomultiplier tube in a right-angle geometry. All fluorescence spectra were corrected for detector response and time-drift and were additionally converted from the recorded wavelength scale $I_f(\lambda_f)$ to a linear energy scale according to $I_f(\nu_f) = I_f(\lambda_f)\cdot\lambda_f^2$.

2.5. Fluorescence Quantum Yields. The quantum yields were measured relative to quinine bisulfate in 0.1 N H_2SO_4 and calculated on the basis of[37]

$$\Phi_f = \Phi_f^0 \frac{n_0^2}{n^2} \frac{OD^0}{OD} \frac{\int I_f(\lambda_f) d\lambda_f}{\int I_f^0(\lambda_f) d\lambda_f} \quad (1)$$

where n_0 and n are the refractive indices of the solvents, OD^0 and OD ($\leq$0.1) are the optical densities, Φ_f^0 (52%)[38] and Φ_f are the quantum yields, and the integrals denote the (computed) area of the corrected fluorescence bands, each parameter for the standard and sample solution, respectively. All quantum yields were determined using a single 1 cm quartz cuvette to minimize instrumental errors. Most values have been remeasured on the same fluorimeter and on a Perkin-Elmer 650-60 and LS 50. The relative experimental error of the quantum yields is ±5%.

2.6. Fluorescence Lifetimes. Synchrotron radiation from the Berlin synchrotron facility BESSY was used as light source in conjunction with an excitation monochromator (Jobin Yvon, ~20 nm band-pass). It delivers a 4.8 MHz pulse train with characteristic pulse widths of 600 ps. Emission was detected using a time-correlated single photon counting setup. It consists of a filter polarizer in magic angle position, emission monochromator (Jobin Yvon, ~20 nm band-pass), and a microchannel plate photomultiplier (Hamamatsu R1564-U-01, 35 ps fwhm) cooled to −30 °C. By means of standard electronics from ORTEC, at most 0.1% of the signals (~5 kHz) were sampled in 1024 channels of a multichannel analyzer (ORTEC-Norland 5590) with a channel width of either 25 or 50 ps. The decays were analyzed by the "least-squares" and iterative reconvolution method on the basis of the Marquardt/Levenberg algorithm, which is implemented in the homemade program "SP" as well as in the commercial global analysis program.[39] The quality of the exponential fits was evaluated by the reduced χ^2 ($\leq$1.2), and the autocorrelation of the residuals was quantified by the Durbin Watson parameter ($1.9 < DW < 2.1$).[40] This reconvolution technique allows an overall time-resolution down to 100−200 ps.

2.7. Quantum Chemical Calculations. CNDO/S-SCI calculations including 49 singly excited configurations have been performed with the QCPE program 333 modified to use the original CNDO/S parametrization[41] and to calculate the excited-state dipole moments. All input geometries were fully optimized in the ground state by the Newton algorithm with the AM1 Hamiltonian within the AMPAC program.[42] In the experiments, we are dealing with solutions which shift the absorption and fluorescence transitions to lower energies ν_a and ν_f. For a rough theoretical estimation of the solvent shifts, the classical Onsager

model[43] is applied, which treats the solvent as a dielectric continuum containing a spherical cavity within which the solute associated with a point dipole resides. With the usual assumption that the initial state is fully stabilized by solvent reorientation and electronic polarization, whereas the final state of the instantaneous electronic transition can only interact with the solvent by electronic polarization, the transition energies for the absorption and fluorescence process are calculated by[44]

$$hc\nu_a = hc\nu_{gas} - f(\epsilon_r)\cdot(\mu_e\mu_g - \mu_g^2) - f(\epsilon_\infty)\cdot(\mu_e^2 - \mu_e\mu_g) \quad \text{(absorption)} \quad (2a)$$

$$hc\nu_f = hc\nu_{gas} - f(\epsilon_r)\cdot(\mu_e^2 - \mu_e\mu_g) - f(\epsilon_\infty)\cdot(\mu_e\mu_g - \mu_g^2) \quad \text{(fluorescence)} \quad (2b)$$

using the well-known Onsager term[43] given in eq 3.

$$f(\epsilon) = \frac{\epsilon - 1}{2\epsilon + 1}\frac{1}{a^3} \quad (3)$$

μ_g and μ_e represent the calculated ground and excited-state dipole moments, h and c are the Planck constant and velocity of light, and ϵ_r and ϵ_∞ denote the static and high-frequency dielectric constant of the solvent. The Onsager cavity radius a is taken as 6×10^{-10} m throughout the paper for the theoretical calculations and the solvatochromic plots. It is calculated by the half-length of the long-molecular axis using the PCMODEL program.[45] The potential energies of the ^{1}CT state $E(^1\text{CT})$ are obtained by combining the ground-state potential from AM1 with the gas-phase excitation energies and adding the solvent stabilization energy for full solvent relaxation[46] according to

$$E(^1\text{CT}) = E_{gas}(S_0) + hc\nu_{gas}(S_0 \rightarrow {}^1\text{CT}) - f(\epsilon_r)\mu_e^2 \quad (4)$$

The ground-state energies $E_{gas}(S_0)$ used are determined relative to the heat of formation (ΔH_f) of the fully optimized geometry (ΔH_f (**I**) = 395 kJ/mol, ΔH_f (**II**) = 366 kJ/mol, ΔH_f (**III**) = 319 kJ/mol). All quantum chemical computations were executed on a HP 735 workstation.

3. Results and Discussion

3.1. Steady-State Spectra. In Figures 1 and 2, the steady-state absorption and fluorescence spectra are shown for **I**−**III** in solvents of different polarity. According to our previous analysis of the absorption spectra, the B band can be assigned to a ^1B_b-type state and the A band to the ^1L_a-type state analogously to the A and B bands in BP.[27,30] The maximum of the first absorption band (CT) of **II** is located 4300 and 8300 cm^{-1} to the red of the corresponding band in 4-dimethylaminobiphenyl[21] and 4-cyanobiphenyl,[19] respectively. This indicates a π-electron delocalization from the dimethylamino to the nitrile group, which is consistent with the assignment to the long-axis polarized transition $1^1A(S_0) \rightarrow 2^1A(^1\text{CT})$.

Regarding the electronic nature (^{1}A or ^{1}B symmetry) and geometrical structure of S_1 after vibrational relaxation, the fluorescence in *n*-hexane (HEX) already contains a wealth of information, because weak solute−solvent interactions in this nonpolar medium do not broaden the vibronic transitions too much, and the stabilization energy of the fluorescent state is due more to intramolecular than to solvation processes. The following information can be extracted from the steady-state fluorescence spectra in HEX (Figure 2):

(i) The fluorescence spectra of all three biphenyl compounds **I**−**III** consist of a strong 0−0 vibronic transition which is not observed in BP.[7] Fluorescence in BP occurs from the forbidden

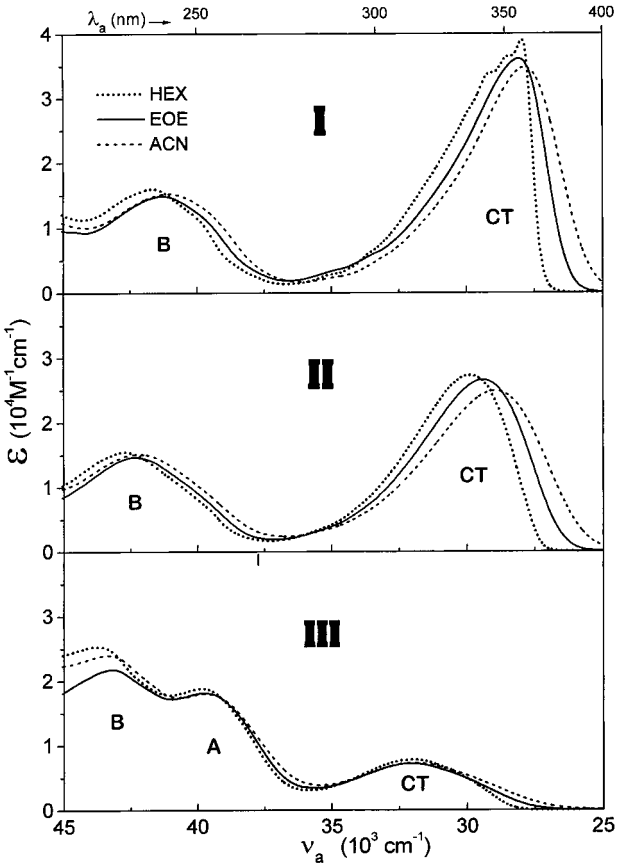

Figure 1. Absorption spectra of **I**−**III** in solvents of different polarity at 298 K.

^1L_b state, which explains the absence of the 0−0 transition. In addition, the degree of polarization (p) of **I**−**III** in EtOH at 77 K (Figure 2) is constant across the fluorescence band and is close to the maximum value of $p = +0.5$ (**I**: $p = +0.47$; **II**: $p = +0.44$; and **III**: $p = +0.48$). Under equal conditions, a value for p of only +0.2 was reported for BP and cyanobiphenyl derivatives.[19] By taking into account the long-axis polarization of the first absorption band,[26] this proves the long-axis polarization of S_1 emission in **I**−**III**, in contrast to BP. Thus, we can suppose that fluorescence of **I**−**III** originates from the allowed $2^1A(^1\text{CT})$ state in a manner similar to that of 4-vinylbiphenyl[8] and fluorene[7] where the observation of the 0−0 transition is also due to a lowest lying long-axis polarized state.

(ii) From a band-shape analysis related to Marcus' ET concept[30,47] or similarly from fitting of the spectral profile to four Gaussian functions (eq 5), the average spacings of the

$$I_f(\nu_f) = \sum_j \frac{\int I_f(\nu_f)d\nu_f}{HW_f^j}\sqrt{2/\pi}\exp\left(-2\frac{(\nu_f - \nu_f^{j,max})^2}{HW_f^{j^2}}\right) \quad (5)$$

progressions for **I** to **III** in HEX are found to amount to (1310 ± 10) or (1320 ± 30) cm^{-1}, respectively. For BP, the spacing is 1000 cm^{-1} and is ascribable to the ring-breathing mode being nontotally symmetric to the C_2 long axis.[8] However, because the fluorescence of BP does not occur from a state with the same symmetry as **I**−**III,** we have to compare the spacings with those of biphenyls showing fluorescence of the long-axis polarized ^1L_a-type. In this case, the progression corresponds to the interannular bond stretching mode being totally symmetric to C_2. Such biphenyls are 4-vinylbiphenyl, *p*-terphenyl, or 4-cyanobiphenyl. All of these compounds possess a spacing[8,19]

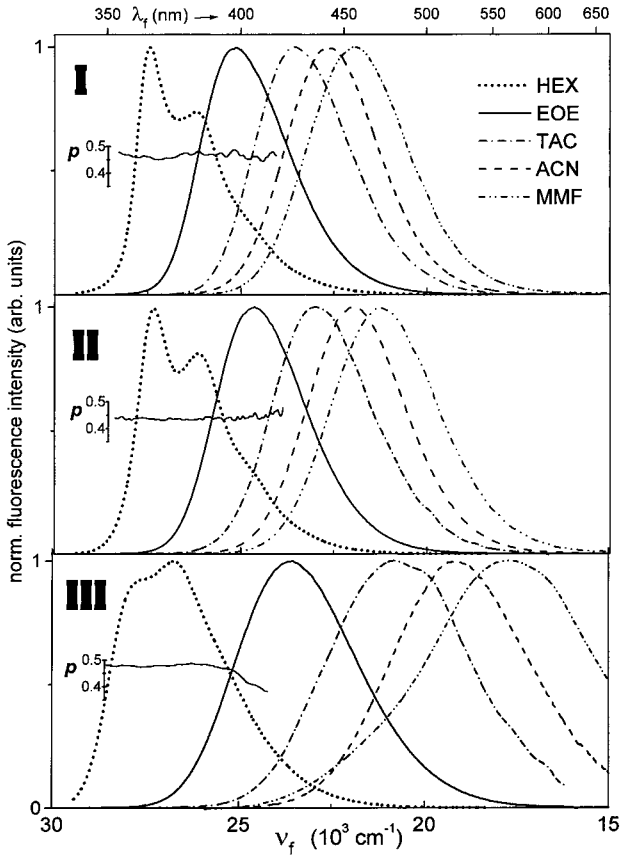

Figure 2. Normalized fluorescence spectra of **I**−**III** in solvents of different polarity at 298 K. The fluorescence polarization spectra $p(\nu_f)$ of **I**−**III** in EtOH at 77 K are also shown. All spectra are obtained by excitation at the absorption maxima. The $p(\nu_f)$ are shifted 2000 cm^{-1} to the blue side to match up the vibronic band positions in EtOH at 77 K with those in HEX at 298 K. The decrease of $p(\nu_f)$ for **III** below the energy of the 0-2 vibronic band is due to long-lived (τ_p = 2.4 s) phosphorescence.

of about 1300 cm^{-1}, which is in excellent agreement with the spacings of **I**−**III** and therewith confirms the ^1L_a character of the emitting ^{1}CT state coupled to the ground state mainly by the totally symmetric interannular bond-stretching vibrational mode.

(iii) In contrast to the absorption bands, the fluorescence bands of **II** and **III** exhibit vibrational structure and considerably narrower half-widths. These observations indicate a narrower conformational distribution in the excited state.

(iv) The increasing Stokes shifts from **I** to **III** point to significant angular relaxations in the excited state of **II** and more extensively in that of **III**.

(v) The intensity of the 0−0 band relative to the second vibronic band is largest (ratio 1:0.74) for the compound **I** restricted to planarity, because the minima of the ground and emitting state are less displaced relative to each other. The high ratio 1:0.81 for the flexible biphenyl **II** also speaks in favor of an angular distribution close to 0°. The lower ratio of 0.93:1 for **III** indicates a larger difference between ground and excited-state minima. This is most probably due to a relaxation from the initial conformational distribution toward an angular distribution with more planar angles $\langle\varphi\rangle$ in S_1 than in S_0. In summary, the steady-state fluorescence in HEX yields evidence that it originates from the allowed 2^1A(^{1}CT) state in which the conformer distribution of **II** and **III** is more planar than in the ground state 1^1A.

The fluorescence in dipolar solvents is structureless and exhibits a solvatochromic red shift with increasing solvent polarity for all D−A biphenyls investigated (Figure 2). Dipole−dipole interactions between solute and solvent are responsible for these large Stokes shifts, and hence the strong solvatochromism proves the sizable ^{1}ET character of the emitting state. Furthermore, the solvatochromism is similar for **I** and **II**, which hints at a planar structure for excited **II** in the dipolar solvents also. In contrast, the solvatochromic red shift for **III** is much more pronounced, indicating a different molecular structure connected with a higher dipole moment in S_1. The quantitative determination of the excited-state dipole moments μ_e (Table 1) is performed using the linear fits (correlation coefficients $r > 0.99$) of the emission maxima ν_f (Table 2) versus the polarity functions $F_2(\epsilon_r,n)$ and $L(\epsilon_r,n)$ according to[48,49] eq 6 and[50−52] eq 7:

$$\nu_f = \nu_f(0) - \frac{2\mu_e(\mu_e - \mu_g)}{hca^3} F_2(\epsilon_r,n)$$

$$\text{with } F_2(\epsilon_r,n) = \frac{2\epsilon_r - 1}{2\epsilon_r + 1} - 0.5\frac{n^2 - 1}{2n^2 + 1} \quad (6)$$

$$\nu_f = \nu_f(0) - \frac{2\mu_e(\mu_e - \mu_g)}{hca^3} L(\epsilon_r,n)$$

$$\text{with } L(\epsilon_r,n) = \frac{\epsilon_r - 1}{\epsilon_r + 2} - 0.5\frac{n^2 - 1}{n^2 + 2} \quad (7)$$

where the static dielectric constants ϵ_r and the refractive indices n of the solvents are taken from ref 53 and the ground-state dipole moments μ_g were calculated with the AM1 method[42] to be 5.72, 5.65, and 5.0 D for **I**−**III**, respectively. The Onsager radius a (6.0×10^{-10} m) is calculated as the half-length of the long-molecular axis without van der Waals radii. The same value for a has been used by different authors for similar D−A biphenyls,[14,54,55] and especially Lahmani et al.,[14] who also investigated compound **II**, used this value and reported practically the same dipole moments for **II**. The polarity function $L(\epsilon_r,n)$ in eq 7 yields dipole moments which are 30% smaller than those obtained with $F_2(\epsilon_r,n)$, because the contribution of the solvent-induced dipole moment is corrected in eq 7 assuming an average polarizability in S_0 and S_1 of about 0.5 a^3 as described elsewhere.[50−52] The higher dipole moments of **III** clearly demonstrate an increased ^{1}ET character in S_1 as compared to **I** and **II**. Both of the latter have similar μ_e and thus contain practically equal ^{1}ET character in S_1. In the framework of the minimum overlap rule,[1,56] these relations of μ_e can be understood by a planar structure of **I** and **II** and a highly twisted molecular structure of **III** associated with orbital localization (cf. Scheme 2).

The absorption and fluorescence spectroscopic data in different solvents are collected in Table 2. The Stokes shifts ($\Delta\nu_{St}$) can be used to estimate the sum of the outer and inner reorganization energy by $\lambda_{sum} = \Delta\nu_{St}/2$ averaged for S_0 and S_1.[47] Such an evaluation leads to a difference between the reorganization energies λ_{sum} of **I** and **II** that remains approximately constant around 1000 cm^{-1} in all solvents. This amount of energy is most probably lost by the intramolecular rotation of **II** toward planarity. In contrast, the Stokes shift of **III** increases immensely with solvent polarity ranging from 5000 cm^{-1} in nonpolar to 14 000 cm^{-1} in highly polar monomethylformamide (MMF), and the corresponding reorganization energies λ_{sum} are always larger than those of **I** and **II** (λ_{sum}(**III**) − λ_{sum}(**I**) = 2000 cm^{-1} in HEX and 4200 cm^{-1} in MMF). The

TABLE 3: Photophysical Properties of I−III at 298 K[a]

	$\int\epsilon d\nu_a$ (M^{-1} cm^{-2})			Φ_f (%)			τ_f (ns)			k_{nr} (10^7 s^{-1})			k_f (10^7 s^{-1})			$k_f/\nu_f^3n^3$ (10^{-7} s^{-1} cm^3)		
solvent	**I**	**II**	**III**	**I**	**II**	**III**	**I**	**II**	**III**	**I**	**II**	**III**	**I**	**II**	**III**	**I**	**II**	**III**
HEX	1.51	1.28	0.38	57	71	35	1.4	1.2	1.2	32	25	55	42	61	30	83	124	60
EOE	1.56	1.35	0.38	83	84	55	1.7	1.7	4.6[b]	10	9	10[b]	50	49	12[b]	128	134	37[b]
ACN	1.58	1.37	0.41	81	79	21	2.1	2.2	7.6	9	10	10	39	35	3	143	142	17
EtOH				84	81	4	2.0	2.2	1.4	8	9	66	42	37	3	146	140	19

[a] Integrated area[60] of the CT absorption band $\int\epsilon d\nu_a$, fluorescence quantum yields Φ_f, fluorescence lifetimes τ_f, nonradiative $k_{nr} = (1 - \Phi_f)/\tau_f$ and radiative rate constants $k_f = \Phi_f/\tau_f$ and reduced radiative rates $k_f/\nu_f^3n^3$. [b] Mean values from biexponential decay due to the equilibrium between two emitting species (see text).

half-widths of the fluorescence bands HW_f are also broader for **III** than for **I** and **II**. This points to the possibility that in **III** a single broad or even two different conformer distributions are fluorescent. Although dual fluorescence bands are not observed, it is not unusual that two sets of similar transition energies of two isomers result in the appearance of only a single band.[57−59] Here, the absence of vibrational structure in the steady-state fluorescence prevents an obvious differentiation between two conformers.

The differences $\Delta_{HEX-ACN}$ between the observed energies in HEX and acetonitrile (ACN) shown in the last lines of Table 2 reveal further interesting aspects. As mentioned above, the differences of the fluorescence energies ν_f, Stokes shifts $\Delta\nu_{St}$, and half-widths HW between nonpolar (HEX) and polar (ACN) solvents are similar for **I** and **II** but different for **III**. Different behavior of **I** and **II** is only observed in the polarity dependence of the absorption energy. For **I**, the absorption energy in ACN with respect to HEX is lower by only 80 cm^{-1}, whereas for **II** this red shift is 10 times larger (780 cm^{-1}). This clearly shows that the ground-state geometries of **I** and **II** are significantly different. **II** must be twisted in the ground state to such an extent that the excited-state Franck−Condon geometry possesses a sufficiently higher dipole moment than **I** to yield the observed polarity-induced absorption red shift. Then the question arises why the absorption red shift for the strongly pretwisted biphenyl **III** is only 100 cm^{-1}, although a large red shift could be expected as a result of the higher excited-state dipole moment. The reason is that in **III**, two absorption transitions of comparable intensity are responsible for the band, one of ^{1}CT and the other one of local partial ^1L_b character.[26] The latter does not change its position with solvent polarity. Partially, this argument may also be valid for compound **I**. In this fluorene derivative, the ^1L_b-type and ^{1}CT transitions can mix, which results in a better allowance of the ^1L_b transition as compared to **II**.[26] Thus, a larger part of the first absorption band might be produced by a nonpolar transition.

We can conclude at this point that **I** and **II** in polar solvents possess a similar conformation in the excited state analogously to the outcome for HEX, whereas in the ground state they differ in their twist angle φ. **III** in polar solvents has quite a different molecular structure than **I** and **II** in the excited state, but the extent of twisting and its difference to the ground state is not yet obvious at this point.

3.2. Photophysics. *3.2.1. Photophysical Evidence for ^1L_a-type Fluorescence*. The photophysical data of **I**−**III** in *n*-hexane (HEX), diethyl ether (EOE), acetonitrile (ACN), and ethanol (EtOH) are collected in Table 3. The integrated absorption intensity $\int\epsilon d\nu_a$, which is proportional to the oscillator strength f, increases only slightly with solvent polarity. This indicates that the electronic and structural nature of the ground and Franck−Condon excited state responsible for the first absorption band does not vary dramatically with polarity. The same holds for the fluorescence of **I** and **II** in dipolar solvents. For these compounds, the fluorescence quantum yields Φ_f stay constant around 80% and the nonradiative rate constants k_{nr} are around 10^8 s^{-1} in all solvents except HEX. The slight variation of the radiative rate constant k_f of **I** and **II** can mainly be traced back to the inherent dependence on ν_f^3 (see eq 9)[61,62] as shown by the near constancy of the reduced radiative rates $k_f/\nu_f^3n^3$.

In apolar HEX, the fluorescence behavior of all three compounds is similar, with the main features that (i) Φ_f is decreased significantly as compared to medium polar EOE and (ii) all lifetimes are comparable, in particular for **II** and **III**. It seems astonishing that the radiative rate k_f for **I** is smaller than for **II** because in the dipolar solvents, **I** and **II** possess very similar k_f values. We can explain the decreased k_f for **I** by a slightly different electronic nature of S_1 in a nonpolar medium. As pointed out elsewhere,[26,30] ^1L_b and ^{1}CT can mix more strongly in compound **I**, which is derived from fluorene with parallel transition moments of its $^1L_b(+)$ and $^1L_a(-)$ states. As a result, the ^{1}CT state in **I** has to share a part of its oscillator strength with the ^1L_b states. In absorption, both ^1L_b and the ^{1}CT states all contribute to the first absorption band, whereas in fluorescence only the emission of the lowest state ^{1}CT can be observed. In polar solvents, on the other hand, the stabilization of the ^{1}CT state leads to a larger energy gap between ^1L_b and ^{1}CT, which can account for reduced mixing between these states connected with an enhancement of the radiative rates for **I**. The polarity dependence of the ^1L_b−^{1}CT mixing can further be substantiated by a comparison with the related biphenyl compound 4-diethylaminobiphenyl (EBA), which possesses a ^{1}CT state somewhat higher lying than in **I**−**III**.[22] The observed larger radiative rate of EBA in ACN ($k_f = 5 \times 10^7$ s^{-1}) with respect to nonpolar cyclohexane (2×10^7 s^{-1}) can be explained similarly to **I** with a stabilization of the fluorescent ^{1}CT state in polar solvents leading to less mixing between the forbidden ^1L_b-type (cf. k_f(BP) = 10^7 s^{-1}) and the allowed ^1L_a-type ^{1}CT transition to the ground state. In any case, the radiative rates k_f and, more meaningfully, the emission energy corrected rates $k_f/\nu_f^3n^3$ for **I**−**III** are 20−150 times higher than for BP ($k_f/\nu_f^3n^3 = 10^{-7}$ s^{-1} cm^3)[8] and thus corroborate the assignment to ^1L_a-type fluorescence independent of the compound and solvent investigated.

3.2.2 Structural and Solvent Dependence of Nonradiative Rates. In all dipolar and aprotic solvents, the nonradiative rates for **I**−**III** are close to 10×10^7 s^{-1}, but in HEX the increased rate constants of about 30×10^7 s^{-1} for **I** and **II** and 55×10^7 s^{-1} for **III** hint at an additional radiationless channel present only in nonpolar surrounding. Although phosphorescence is not observed in the liquid phase of the solvents, this channel is most probably due to intersystem crossing (ISC).[30] A similar behavior has recently been found for 9,9′-bianthryl where the ISC rate in HEX is ∼2 times larger than in EOE and ∼4 times larger than in ACN.[63] This was explained with a thermally activated ISC process to the second triplet state (T_2), which becomes relatively higher lying than the solvent-stabilized S_1 with

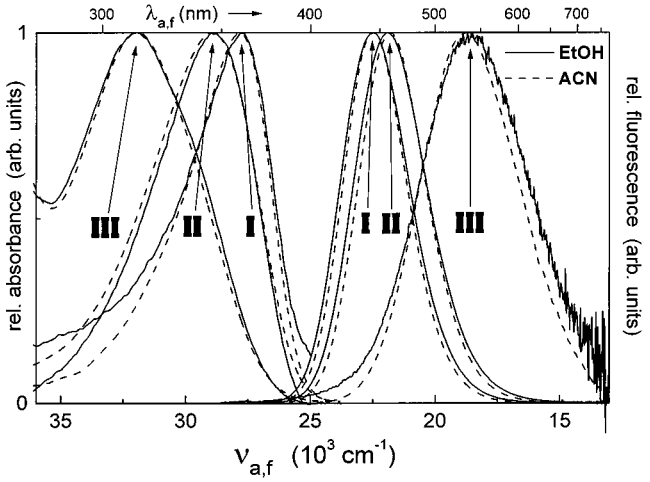

Figure 3. Normalized absorption and fluorescence spectra of **I**−**III** in protic ethanol and aprotic acetonitrile at 298 K. The coinciding maxima and similar shapes of the spectra in both (≈equipolar) solvents indicate that hydrogen bonding occurs neither in the ground nor in the emitting state. The high noise in the fluorescence spectrum of **III** in EtOH (together with the shortened lifetime) reveals the deactivation to a nonradiative excited species as a result of protic solvent interaction.

increasing polarity. The level reversal between S_1 and a triplet state may also take place in **I**−**III** when switching from HEX to polar solvents.[30] The suggestion of an additional ISC channel in HEX is further supported by the higher nonradiative rate for **III** than for **I** and **II**. Note also that the emission polarization spectrum of **III** at 77 K, shown in Figure 2, is contaminated by the perpendicular polarized phosphorescence contribution in the 0−2 vibronic band as evidenced by the long lifetime of 2.4 s. In contrast to the $^1\pi\pi^*$ singlet states, in the triplet $^3\pi\pi^*$ states the transition moments are usually polarized perpendicular to the π-system. Because the angle between the transition moment directions of the singlet transition in one phenyl ring is less perpendicular to that of the triplet transition in the other ring for **III** than for **I** and **II**, stronger excitonic interactions between singlet and triplet excitations should occur for the more twisted compound **III** with the consequence of a faster ISC rate. Such a twist angle dependent triplet yield has also been reported for BP.[7,64]

The behavior of **III** in EtOH is rather outstanding. Whereas all photophysical data are equal for **I** and **II** in ACN and EtOH, only the radiative rate is the same in both solvents for **III**. Quantum yield and lifetime are strongly reduced, which is the result of an additional radiationless channel resulting in a ∼7-fold increase of the k_{nr} rates.

This can be further discussed with the aid of Figure 3, which shows the comparison of the absorption and fluorescence spectra of **I**−**III** between protic EtOH and aprotic ACN. Both solvents are of comparable polarity ($F_2(\epsilon_r,n) = 0.38$ for EtOH and 0.39 for ACN). Absorption and fluorescence band shapes and maxima and their change with twist angle from **I** to **III** are similar in EtOH and ACN. From the similarity of the absorption spectra in the two solvents, it can be deduced that there is no specific ground-state complexation with EtOH, and likewise the similarity of the fluorescence spectra indicates that the fluorescent species is the same in EtOH and ACN. However, a remarkable reduction of the fluorescence quantum yield of **III** in EtOH (Table 3) as testified by a lower S/N ratio (Figure 3) is the result of a dynamic quenching process to a nonfluorescent product in the excited state of **III**. The effect of hydrogen bonding with the consequence of the formation of a nonfluorescent ^{1}CT state engaged in an excited hydrogen bonded pair

SCHEME 3

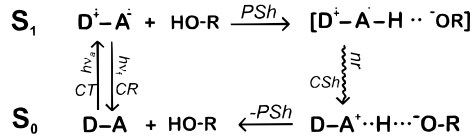

is a well-known and frequently encountered phenomenon.[16,65−67] Although a 1:1 complex with the dimethylamino group has been reported leading to a nonfluorescent channel,[66] in our case, a ground-state complexation between the dimethylaminonitrogen and EtOH can be ruled out because upon addition of EtOH to a solution of **III** in ACN, the absorption spectrum remains unchanged, whereas the fluorescence quantum yield strongly decreases by the dynamic fluorescence quenching.

Moreover, in the related D−A biphenyls 4-*N*,*N*-dimethylanilino-pyrimidine[16] and 4-*N*,*N*-dimethylamino-4′-formyl-biphenyl[18] in which quenching hydrogen bonding has also been observed, complexation at the acceptor unit (more precisely at the ring nitrogen and the carbonyl oxygen) could be shown. Therefore, in the case of **III**, a specific hydrogen bonding interaction in S_1 with the negatively charged acceptor benzonitrile unit, in particular with the nitrile group, is proposed. The question remains why the quenching does not appear in the D−A biphenyls **I** and **II**. In the carbonyl and pyrimidine biphenyl derivatives that are related to **II**, the hydrogen bonding interaction is stronger and takes place already in the ground state, indicated by a shift of the absorption spectra in EtOH with respect to ACN. The difference of **I** and **II** as compared to **III** in S_1, however, can be understood by a strongly delocalized π-electronic structure for **I** and **II** with the central bond of partial double-bond character in the valence-bond description as denoted in eq 8a, and in contrast, by a different biradicaloid electronic structure for **III** (eq 8b).

$$(\mathbf{I},\mathbf{II}) \quad \mathrm{D{-}A} \xrightarrow{h\nu} \mathrm{D^{+}{=}A^{-}} \tag{8a}$$

$$(\mathbf{III}) \quad \mathrm{D{-}A} \xrightarrow{h\nu} \mathrm{D^{\bullet+}{-}A^{\bullet-}} \tag{8b}$$

This biradicaloid structure (eq 8b) is reached only for a strongly twisted geometry and can explain the quenching process in the excited state of **III** by the reaction cycle in EtOH shown in Scheme 3. The proposed scheme involves a competition in the photoexcited ^{1}CT state between (i) radiative (and nonradiative) charge recombination (CR) and (ii) a proton shift (PSh) from ethanol to the acceptor side of **III** inside the solvent cage. Channel (ii) leads to a positively charged biradicaloid form of the donor−acceptor biphenyl **III**. Such cations are widely known for their fast radiationless decay to the ground-state accompanied by an intramolecular charge shift (CSh).[17,68,69] In the ground state, the basicity of the acceptor unit is drastically reduced and hence, the proton captured in S_1 is released in S_0 (−PSh).[30]

3.2.3. Ratios of Radiative Rate Constants as Indicators for Angular Relaxations. The central observation of this work is that the strong decrease of the radiative rate k_f ($= \Phi_f/\tau_f$) with increasing polarity occurs only for **III**. k_f is 10 times higher in HEX than in ACN or EtOH. To exclude the effect of the ν_f^3 dependence on the radiative rate k_f according to eq 9,[61,62] a

$$k_f = \frac{64\pi^4}{3h} n^3 \nu_f{}^3 M_f^2 \tag{9}$$

decrease of the reduced radiative rates $k_f/n^3\nu_f^3$ being directly proportional to the square of the fluorescence transition moment M_f is also confirmed in Table 3. As compared to **I** and **II**, which

TABLE 4: Ratios of Fluorescence Rate to Strickler−Berg Rate Constants k_f/k_f^{SB}

solvent	I	II	III
HEX	0.71	1.33	2.28
EOE	1.03	1.32	1.40
ACN	1.13	1.33	0.60

show rather no polarity dependence of the reduced radiative rates $k_f/n^3\nu_f^3$, a different and polarity-dependent excited-state process must take place in **III**.

A change of the electronic or molecular structure between the absorption and fluorescence process can readily be evaluated by a comparison of the fluorescence rate constant k_f with the Strickler−Berg rate constant k_f^{SB} obtained from the absorption spectra using eq 10, where the integrated absorption spectrum is given by eq 11.[6,70]

$$k_f^{SB} = \frac{8\pi c 10^3 \ln 10}{N_L} n^2 \nu_f^3 \int \epsilon(\nu_a) d \ln \nu_a \qquad (10)$$

$$\int \epsilon(\nu_a) d \ln \nu_a = \frac{8\pi^3 N_L n}{3hc 10^3 \ln 10} M_a^2 \qquad (11)$$

After substitution of eq 11 into eq 10, it can be derived that the ratio k_f/k_f^{SB} is independent of ν_f and n and equal to the ratio of the fluorescence to the absorption squared transition moment: $k_f/k_f^{SB} = M_f^2/M_a^2$. Hence, if no change of the electronic or molecular structure takes place in S_1, a ratio of unity must be obtained.

The ratios k_f/k_f^{SB} are shown in Table 4. As it has been worked out so far that emission occurs only from the allowed ^1L_a-type $^1CT(2^1A)$ state, we can discuss the rate ratios k_f/k_f^{SB} mainly on the basis of conformational changes in S_1. The ratios k_f/k_f^{SB} of **I** in EOE and ACN are both close to unity, indicating similar conformers in S_0 and S_1. The deviation in HEX has been explained above by electronic coupling effects between close lying ^1L_b- and ^1L_a-type states occurring only in **I**. For **II**, all k_f/k_f^{SB} ratios amount to 1.33, which means that the conformer distribution in S_1 (a) is the same in all solvents, (b) is different from that in S_0, and (c) has transition dipole moments (M_f in eq 9) higher than those in S_0 (M_a in eq 11). Two further observations confirm that mainly angular relaxations are detected by the ratios: (i) only the ratio of the planar model compound **I** is 1 and (ii) the energy corrected rates $k_f/\nu_f^3 n^3$ in Table 3 (except in HEX) are very similar for **I** and **II**. The ratio of 1.33 for **II** is then indicative of a fast relaxation of **II** toward full planarity in S_1.

In contrast to **I** and **II**, the pretwisted biphenyl **III** shows solvent-dependent k_f/k_f^{SB} ratios as a result of varying k_f values. Consequently, the fluorescence of **III** is most probably connected with polarity-dependent rotamer distributions. In the nonpolar solvent HEX, the large k_f/k_f^{SB} ratio of 2.3 points to the same process as for **II**, i.e., an angular relaxation in S_1 to conformations with transition probability higher than that in S_0, consistent with a more planar geometry. In the highly polar ACN, conversely, an average conformation in S_1 is observed with a lower transition probability as compared to the conformational distribution in S_0. Let us denote the fluorescent species mainly observed in HEX as **CT** (with a similar photophysical behavior, as for **I** and **II**) and that observed at lower energies in ACN as the more relaxed species **CTR** (considerably less emissive than **CT**). The intermediate k_f/k_f^{SB} ratio in medium polar EOE ranges between HEX and ACN and can either be the result of another single conformer distribution different from

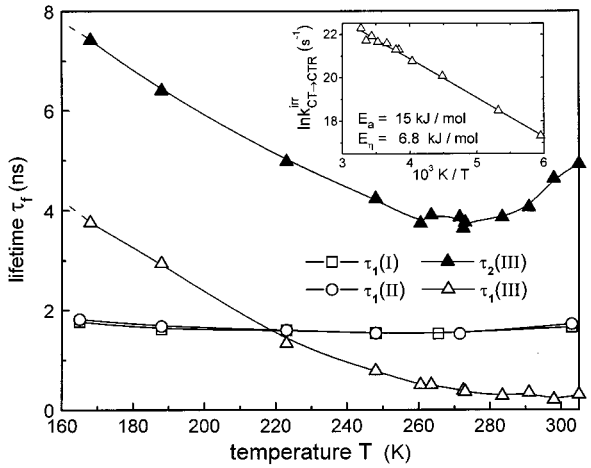

Figure 4. Fluorescence lifetimes in diethyl ether vs temperature as obtained from monoexponential fits of the fluorescence decays for **I** (-□-) and **II** (-○-) and biexponential fits for **III** (τ_1: -△-, τ_2:-▲-). The Arrhenius plot for **III** using the lifetime data of $\tau_1(T)$ is shown as an inset. τ_1 at 160 K is taken as the reference lifetime τ_0(CT) according to eqs 3−16. The regression coefficient is 0.99, and the preexponential factor amounts to 1.5 ps^{-1}. The derived activation barrier E_a is more than twice as high as that for the solvent mobility E_η of EOE, pointing to an intramolecular energy barrier between **CT** and **CTR**.

CT and **CTR** or be due to an equilibrium of both species. In the equilibrium case of such differently emissive species, biexponential fluorescence decays should be observable. Indeed, all decays used for Table 3 are perfectly fitted with single-exponential functions ($\chi^2 = 1.05 \pm 0.05$, DW $= 2 \pm 0.1$) without emission wavenumber dependence of the lifetimes within the error limits of the time-resolution, with the exception of the decay of **III** in EOE. In this case only, a second short time component was necessary to improve the fitting parameters χ^2/DW from 1.29/1.62 to the acceptable values 1.1/2.01. The lifetime of this fast component at 298 K is near the limit of the time-resolution ($\geq$100 ps) of the experimental equipment.

3.2.4. Excited State Conformational Equilibrium for III. The lifetimes in EOE are plotted versus temperature in Figure 4 to obtain a more reliable value for the fast time constant at room temperature by extrapolation. The short lifetime τ_1 derived in this manner is around 200 ps. On the contrary, the fluorescence decays of **I** and **II** can be described by monoexponential fits over the whole temperature range from 168−313 K.[71] Further, the lifetimes of **I** and **II** are equal and practically do not change across the whole temperature range, supporting the view that emission of **I** and **II** occurs from a single and planar distribution of rotamers within the ^1CT potential surface. The biexponential behavior of **III**, however, clearly demonstrates the emission from two different conformer distributions, one of which is assigned to the **CT** species (τ_1(160 K) = 4.3 ns) and the other to the **CTR** species (τ_2(160 K) = 7.3 ns). This interpretation is confirmed by the strong and continuous wavenumber dependence of the amplitudes of both lifetimes as shown in Figure 5. It is important to note that in the low energy tail of the fluorescence spectra (at $\nu_f < 20 \times 10^3$ cm^{-1} in Figure 5) the amplitudes α_1 of the short time component τ_1 become negative. By taking into account the results of time-resolved absorption, which point to an initial population of more planar conformers associated with the **CT** species after the primary charge-transfer step within 5 ps,[31] it can be concluded that the **CT** distribution undergoes a net photoreaction to the **CTR** distribution and hence, the excited-state (decay) behavior has to be interpreted with a dynamic equilibrium as illustrated in Scheme 4. Consequently, the observed two lifetimes τ_1 and τ_2 are not

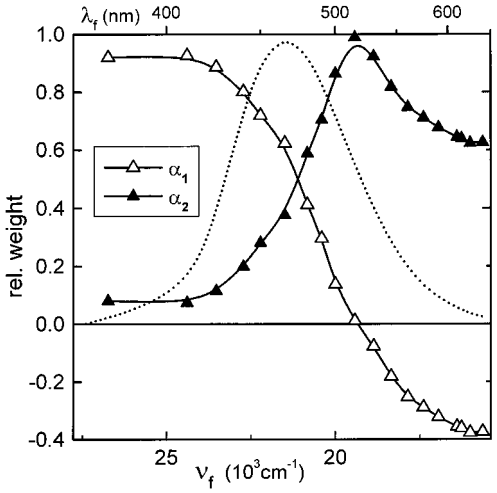

Figure 5. Relative amplitudes $\alpha_1(\nu_f)$ and $\alpha_2(\nu_f)$ of the globally fitted fluorescence decay traces $I_f(\nu_f,t) = \alpha_1(\nu_f)\exp(-t/\tau_1) + \alpha_2(\nu_f)\exp(-t/\tau_2)$ of **III** in EOE at 188 K. Using the linked lifetimes $\tau_1 = 2.9$ ns and $\tau_2 = 6.4$ ns for 20 decay curves at different wavenumbers, a global $\chi_{glo}^2 = 1.17$ is achieved. The steady-state fluorescence spectrum $I_f(\nu_f)$ is plotted as a dotted line.

SCHEME 4. Excited-State Dynamic Equilibrium between Two Conformationally Different Charge Transfer Species[a]

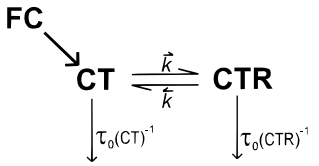

[a] The assumption that the more emissive CT species is primarily populated instead of CTR is based on the initial relaxation toward planarity on a picosecond timescale as revealed by the transient absorption experiments in ref 31 and the calculated S_1 twist potentials for small solvent stabilization (Figure 9).

corresponding to the single decay times (τ_0) of **CT** and **CTR** but are a function of the forward and back reaction rate constants $k_{CT\rightarrow CTR}$ and $k_{CT\leftarrow CTR}$ and of the total deactivation rates X and Y of **CT** and **CTR** according to the well-known Birks eq 12.[61]

$$\tau_{1,2}^{-1} = \frac{1}{2}(X + Y \pm \sqrt{(X-Y)^2 + 4k_{CT\rightarrow CTR}k_{CT\leftarrow CTR}}) \quad (12)$$

$$X = \tau_0(CT)^{-1} + k_{CT\rightarrow CTR} \qquad Y = \tau_0(CTR)^{-1} + k_{CT\leftarrow CTR}$$

These equations can be used to derive that the decrease of the lifetimes τ_1 and τ_2 with increasing temperature (Figure 4) is due to the acceleration of the equilibration rates $k_{CT\rightarrow CTR}$ and $k_{CT\leftarrow CTR}$, respectively.

If the possible back reaction **CT**←**CTR** is neglected in a first approximation,[72] then τ_1^{-1} simplifies to X, i.e., to the sum of the photoreaction rate $k_{CT\rightarrow CTR}$ and the inverse of the intrinsic **CT** fluorescence lifetime $\tau_0(CT)^{-1}$. The latter can be replaced by τ_1 at the glass transition temperature ($T_g \approx 160$ K) where $k_{CT\rightarrow CTR}$ is negligibly small. Under these assumptions, the activation barrier separating **CT** from **CTR** can directly be obtained from the Arrhenius plot (eq 13) shown as an inset in

$$\ln k_{CT\rightarrow CTR}^{irr} = \ln(\tau_1^{-1}(T) - \tau_0(CT)^{-1}) = -\frac{E_a^{irr}}{RT} + \text{const} \quad (13)$$

Figure 4. It has to be kept in mind that the derived activation barrier E_a^{irr} is representative for the case of an irreversible reaction from **CT** to **CTR**[72] and that it contains both the contributions from the intrinsic activation barrier $E_i^{\#}$(CT→CTR) and from a "dynamic barrier" E_η induced by the solvent viscosity.[73] Nevertheless, the obtained activation barrier E_a^{irr} of 15 kJ/mol (1250 cm^{-1}) is considerably higher than the barrier for the solvent mobility of EOE ($E_\eta = 6.8$ kJ/mol) and hence strongly supports the presence of an intrinsic barrier and the coexistence of two distinct conformer species denoted as **CT** and **CTR**. It is noteworthy that the barrier obtained is even around 4 times higher than that reported for DMABN in EOE ($E_a = 4.0$ kJ/mol).[74]

At room temperature in EOE, the two distributions are in fast equilibrium, and in this case of thermodynamic control ($k_{CT\rightarrow CTR} \gg \tau_0(CT)^{-1}$, $k_{CT\leftarrow CTR} \gg \tau_0(CTR)^{-1}$) eq 12a and b can be simplified to

$$\tau_1^{-1} = k_{CT\rightarrow CTR} + k_{CT\leftarrow CTR} \quad (14a)$$

$$\tau_2^{-1} = f_{CT}\tau_0(CT)^{-1} + (1 - f_{CT})\tau_0(CTR)^{-1} \quad (14b)$$

$$f_{CT} = k_{CT\leftarrow CTR}/(k_{CT\rightarrow CTR} + k_{CT\leftarrow CTR}) \quad (14c)$$

where f_{CT} is the fraction of **CT** at equilibrium. The measured mean lifetime $\langle\tau_f\rangle$ ($= \tau_2$) in EOE (Table 3) at room temperature is therefore a weighted average of the intrinsic **CT** and **CTR** decay times $\tau_0(CT)$ and $\tau_0(CTR)$ yielding an intermediate value between that of HEX (mainly strongly emissive **CT** species) and that of ACN (mainly less emissive **CTR** species). Assuming a fraction of 100% **CT** in HEX and 100% **CTR** in ACN and correcting for the solvent dependence of k_{nr}, n^3, and ν_f^3 to the conditions in EOE, the intrinsic lifetimes $\tau_0(CT) = 3.5$ ns and $\tau_0(CTR) = 6.6$ ns at 298 K can be derived.[75] With these values the fraction of **CT** (f_{CT}) in EOE is calculated to be 47% from eq 14b, consistent with an equilibrium constant $K_{eq} \approx 1$ and with a reaction free energy change ΔG around zero in EOE at 298 K. This finding is well understandable with the similarity of the fluorescence energies of the **CT** and **CTR** species.

3.3. Theoretical Calculations. In this section, after some basic considerations regarding twist potentials, CNDO/S-CI calculations are employed to investigate whether different rotamers can be responsible for the fluorescent species **CT** and **CTR**. Moreover, the calculated properties of the two lowest lying states ^1L_b and ^1CT are compared to clarify that emission is due to a purely ^1L_a-type ^1CT state.

3.3.1. Twist Potentials in S_0. In general, twist potentials of biaryls, which are calculated here by AM1 for **II** and **III** in S_0 (Figure 6), result from an energetical compromise between the π-resonance energy (minimum at $\varphi = 0°$) and the sterical potential (minimum at $\varphi = 90°$) mainly induced by the substituents in the ortho positions. Because this sterical hindrance of free intramolecular rotation is enhanced in **III** by the methyl groups, the calculated (intrinsic) barrier at $\varphi = 0°$ is much higher for **III** ($E_i^{\#}(0°) = 66$ kJ mol^{-1}) than for **II** ($E_i^{\#}(0°) = 5.2$ kJ mol^{-1}), whereas at $\varphi = 90°$, it is lower for **III** ($E_i^{\#}(90°) = 0.5$ kJ mol^{-1}) than for **II** ($E_i^{\#}(0°) = 7.7$ kJ mol^{-1}). Because both biphenyls possess C_2 symmetry,[76] the potentials and the corresponding Boltzmann rotamer distributions $\eta(\varphi)$ (eq 15) are symmetric to $\varphi = 0°$ and $\varphi = 90°$. In the following, we therefore refer only to the twist region $\Delta\varphi = 0-90°$. This means that we have only a single distribution of equivalent rotamers around the equilibrium angle $\varphi_{eq} = 39°$ for **II** and $\varphi_{eq} = 78°$ for **III**. In addition, it should be noted that φ_{eq} differs from the mean twist angle $\langle\varphi_\eta\rangle$ (eq 16) which is convoluted

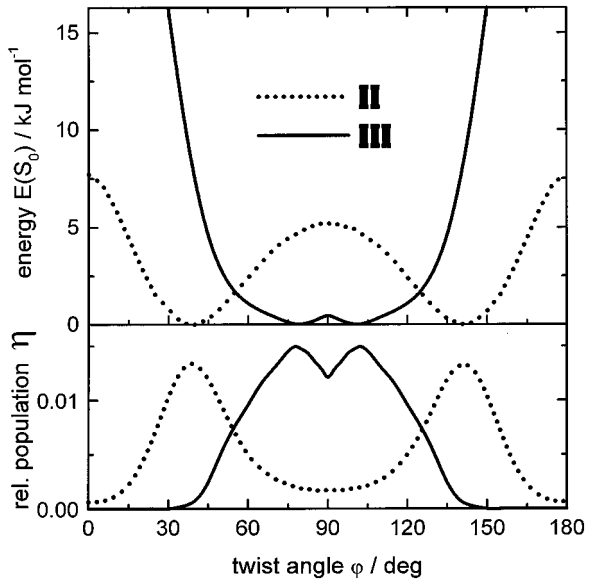

Figure 6. Ground-state twist potentials derived from AM1 optimizations (upper panel) and the corresponding rotational distributions $\eta(\varphi)$ calculated for 298 K according to the Boltzmann eq 15 (lower panel) for **II** (dotted line) and **III** (solid line).

$$\eta(\varphi) = \frac{e^{-E(\varphi) - E(\varphi_{eq})/RT}}{\int_{0°}^{180°} e^{-E(\varphi) - E(\varphi_{eq})/RT} d\varphi} \quad (15)$$

$$\langle \varphi_\eta \rangle = \int_{0°}^{180°} \varphi \eta(\varphi) d\varphi \quad (16)$$

with the distribution function $\eta(\varphi)$ and therefore gives a better representation for experimentally obsevable values ($\langle \varphi_{exp} \rangle$). In S_0, $\langle \varphi_\eta \rangle$ equals 34.5° for **II** and 72° for **III** and depends only slightly on the solvent polarity (using $E_{ACN}(\varphi) = E_{gas}(\varphi) - f(\epsilon_r)\mu_g^2$ for the solvent-stabilized ground-state energy in acetonitrile (cf. eq 4) in eq 15, a value for $\langle \varphi_\eta \rangle$ only 0.5° more planar for both **II** and **III** is obtained.

3.3.2. Electronic Nature of S_1. The calculated dipole moments μ, the absorption and fluorescence transition energies ν_a and ν_f in diethyl ether, and the reduced radiative rates k_f/ν^3 of the ^{1}CT and ^1L_b states are plotted as a function of the twist angle φ for the flexible biphenyl **II** in Figure 7a−c and for the sterically hindered derivative **III** in Figure 8a−c. The single symbols at 0° in Figure 7a−c indicate the data for the D−A fluorene **I**, which serves as the planar model compound.

Because of the calculated low dipole moments (Figure 7a and 8a) of the ^1L_b state its stabilization by the solvent is negligible. In contrast to ^1L_b, the ^{1}CT state is already strongly stabilized in the calculated absorption process but distinctly more in the fluorescence transition (Figure 7b and 8b). As a result, the ^{1}CT state of **II** becomes the lowest excited singlet state at twist angles $\varphi = 0°-50°$ in absorption and at $\varphi = 0°-70°$ in fluorescence (Figure 7b). However, the twist angle region for the pretwisted biphenyl **III** is restricted to values of φ above 20° in S_1 and S_0 as a result of the sterical strain (in S_0: $E(20°) = 30$ kJ mol^{-1} = 2500 cm^{-1}). In the accessible angular region ($\varphi > 20°$), the calculated ^{1}CT state of **III** is not sufficiently stabilized to become the lowest lying state in absorption. ^1L_b and ^{1}CT are very close lying under these conditions, in agreement with the large absorption contribution of a perpendicularly polarized transition within the first absorption band.[26] The situation changes when solvent relaxation in S_1 is switched on. The ^{1}CT transition is then the lowest one across the whole angular range and should be responsible for the fluorescence.

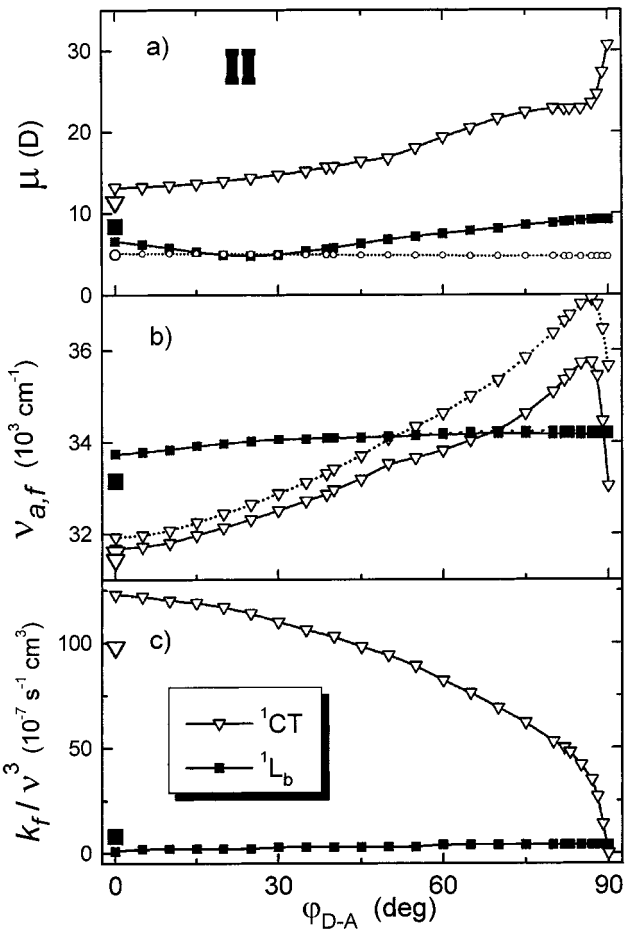

Figure 7. Twist angle dependent results of the CNDO/S-SCI calculations using fully optimized ground-state geometries of **II** (and **I** at 0°) derived from AM1. The calculated properties of the two lowest lying excited states ^{1}CT (-▽-) and ^1L_b (-■-) are compared as a function of the interannular twist angle φ: (a) permanent excited-state dipole moments μ, (b) absorption (ν_a symbol connected with dashed lines) and fluorescence (ν_f symbols connected with full lines) transition energies in diethyl ether calculated from eqs 2a,b, and (c) reduced radiative rates calculated from eq 9. The ground-state dipole moments for **II** (-○-) and all corresponding results for **I** (larger single symbols at $\varphi = 0°$) are also shown.

By taking also into account that the experimental dipole moments (**I**−**III**: $\mu_e = 15-19$ D using $L(\epsilon,n)$) and reduced radiative rates $k_f/\nu_f^3 n^3$ (**I**: 80−150 10^{-7} s^{-1} cm^3; **II**: 120−140 10^7 s^{-1} cm^3; **III**: 15−60 10^{-7} s^{-1} cm^3) given in Table 3 can be well correlated with those of the ^{1}CT state (Figure 7bc and 8bc) but are considerably larger than those calculated for the ^1L_b states ($\mu_e < 10$ D, $k_f/\nu^3 < 10^{-8}$ s^{-1} cm^3) irrespective of the compound or twist angle φ, the assignment of the observed emission to the ^{1}CT(2^1A) state remains unambiguous. Besides, a CI analysis of the calculations reveals that the comparably low fluorescence rate of **I** in HEX follows from strong mixing between the ^1L_b-type and ^{1}CT state. Therefore, the calculated fluorescence rate of **I** is smaller than that of **II** at 0° (Figure 7c). In the polar solvents, mixing between ^1L_b and ^{1}CT is decreased, leading to higher emission rates similar for **I** and **II** at 0° (Table 3).

3.3.3. Molecular Structure in S_1. In the Experimental Section, it was suggested that the similar fluorescence properties (band half-widths, dipole moments, radiative rates, and transition energies) of **I** and **II** point to a planar structure of **II** in S_1. Indeed, Figure 7 supports this view, since the calculated dipole moments and fluorescence energies are nearly identical for **I**

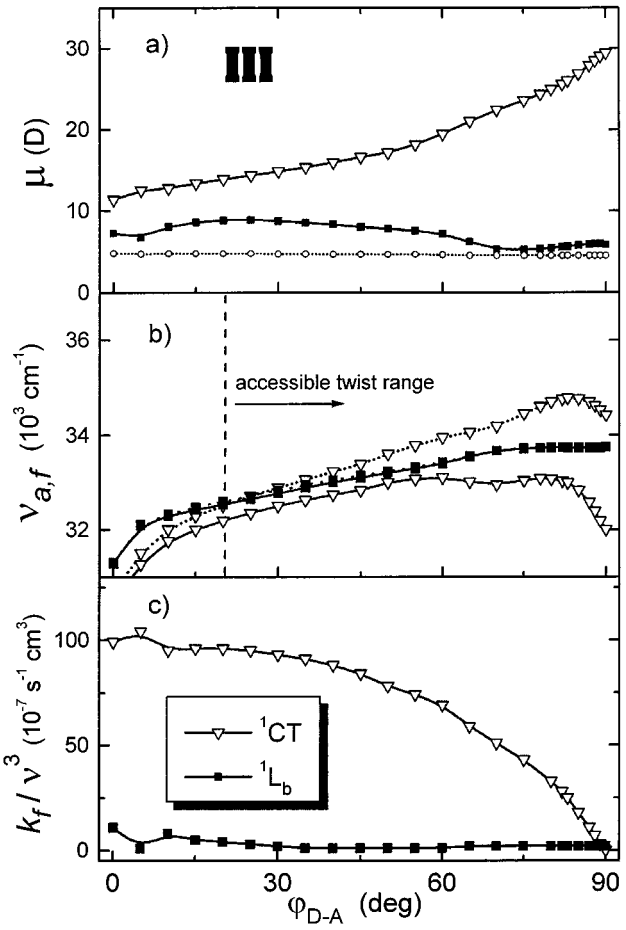

Figure 8. Twist angle dependent results of the CNDO/S-SCI calculations using fully optimized ground-state geometries of **III** derived from AM1. The calculated properties of the two lowest lying excited states ^{1}CT (-▽-) and ^{1}L$_b$ (-■-) are compared as a function of the interannular twist angle φ: (a) permanent excited-state dipole moments μ, (b) absorption (ν_a symbol connected with dashed lines) and fluorescence (ν_f symbols connected with full lines) transition energies in diethyl ether calculated from eqs 2a,b (c) reduced radiative rates calculated from eq 9. The ground-state dipole moments for **III** (-○-) are also shown.

and **II** at $\varphi = 0°$. Furthermore, the calculated fluorescence energy difference between a twisted ($\varphi \approx 35°$) and the planar rotamer (Figure 7b) is in excellent agreement with the additional reorganization energy ($\lambda_{sum} = \Delta\nu_{St}/2$) of 1000 cm^{-1} for **II** as compared to **I** (Table 1). This solvent-independent energy loss of **II** in S_1 can therefore be attributed to the intramolecular rotation.

Concerning the initial (Franck−Condon) geometry, we can explain the slightly stronger solvatochromic shift, larger transition energy, and lower intensity of the first absorption band (Figure 1) for **II** as compared to **I** on the basis of Figure 7 by a less planar molecular structure in S_0 associated with (a) a higher Franck−Condon S_1 dipole moment, (b) larger absorption energy, and (c) smaller radiative rates (eq 9). These comparisons between theoretical and experimental results underline that **II** relaxes in S_1 from a medium twisted toward a planar rotamer distribution.

For **III**, the polarity-dependent radiative rates (Tables 3 and 4) and the biexponential decay behavior in EOE (Figures 4 and 5) lead to the proposal of the coexistence of two electronically different conformer distributions, even though only single, but broad, emission bands are observed (Figure 2). To explain this discrepancy, we have to note that the transition energies in the solvent-stabilized case are modified by two counteracting energy contributions (eq 2). With increasing twist angle φ, the pure electronic energy increases but the stabilizing solvation energy also increases as a result of the larger dipole moments for higher twist angles φ (Figure 8b). As a consequence, the fluorescence energies of the rotamers in the accessible twist range of **III** are very similar in EOE, which prevents the occurrence of two separated emission bands. To evaluate whether both counteracting energy contributions result in either a relatively flat potential of the ^{1}CT state connected with a broad angular distribution or a double minimum potential with two peaks of the conformer distribution, the ^{1}CT twist potentials of **II** and **III** are calculated in different solvents applying classical Onsager theory (eq 4).

Indeed, only for the gas phase, the ^{1}CT twist potentials (Figure 9) of **II** and **III** exhibit a single minimum at an angle φ_{eq} which is 30°−40° smaller as compared to the calculated equilibrium angle in S_0 (Table 5). With increasing solvent polarity, this ^{1}CT energy minimum slightly shifts to higher twist angles $\varphi_{eq}(^1CT)$ and a second energy minimum evolves for the perpendicular geometries. For **II** in EOE, the barrier $E_i^{\#}(90)$ from the minimum at planarity to the steep minimum at 90° is calculated to be very high (45 kJ), which can explain why a second twisted rotamer distribution is not populated and not observed in all experiments with **II**. In the case of **III** in EOE, the calculated double minimum potential is associated with a low barrier of 2 kJ (170 cm^{-1}). The barrier $E_i^{\#}(90°)$ theoretically found in HEX (14 kJ) agrees well with the activation barrier E_a^{irr} (Figure 4) found experimentally in EOE (15 kJ).

Some general comments on the shape of the potential curves have to be noted. All potential curves obtained are based on the wave function of the ^{1}CT state in the gas phase. However, as a result of energy stabilization of the ^{1}CT state in solution, its electron transfer (^{1}ET) character[29] is enhanced at the expense of the weakly polar ^1L_a character.[30] As the ^{1}ET character for the perpendicular geometries is already nearly 100% (minimum overlap rule)[56] without solvent stabilization, it can easily be deduced that the solvent-induced increase of electron-transfer character is stronger for medium twisted than for more perpendicular rotamers. This will lead to a flattening of the dipole moment dependence on the twist angle φ (Figure 7a and 8a). As a result of the solvent interaction, the energy minima are expected to be broader and located at more planar angles φ than calculated with the gas-phase dipole moments μ in Figure 7a and 8a. A shift and decrease of the barrier $E_i^{\#}(90°)$ might also occur. In this sense, the potentials for **III** already give a more realistic representation, because the ^{1}ET weight at a given value of φ is intrinsically higher than for **II** because of the inductive effect of the two methyl groups.[26] A detailed analysis of the solvent effects on the ^{1}CT wave function indicates only minor effects on the torsional pathways in S_1. Although it has also been verified using idealized geometries and selected geometries optimized in the excited state that reasonable structural changes, e.g., planarization of the pyramidalization angle of the dimethylamino nitrogen or shortening of the interannular bond lengths, have negligible influence on the essential shape of the excited state twist potentials (e.g., the occurrence of two minima) and on the properties shown in Figures 7 and 8, their possible influence has to be mentioned. Thus, the potential curves in Figure 9 and the derived twist angles and barriers in Table 6 should mainly be regarded relative to each other to explain the excited-state structural relaxations. Nevertheless, the calculated potentials in combination with the experimental results obviously confirm that in the excited state (a) **II** relaxes to a planar structure irrespective of the solvent as a result of the absence of a barrier toward planarity ($E_i^{\#}(0°) =$

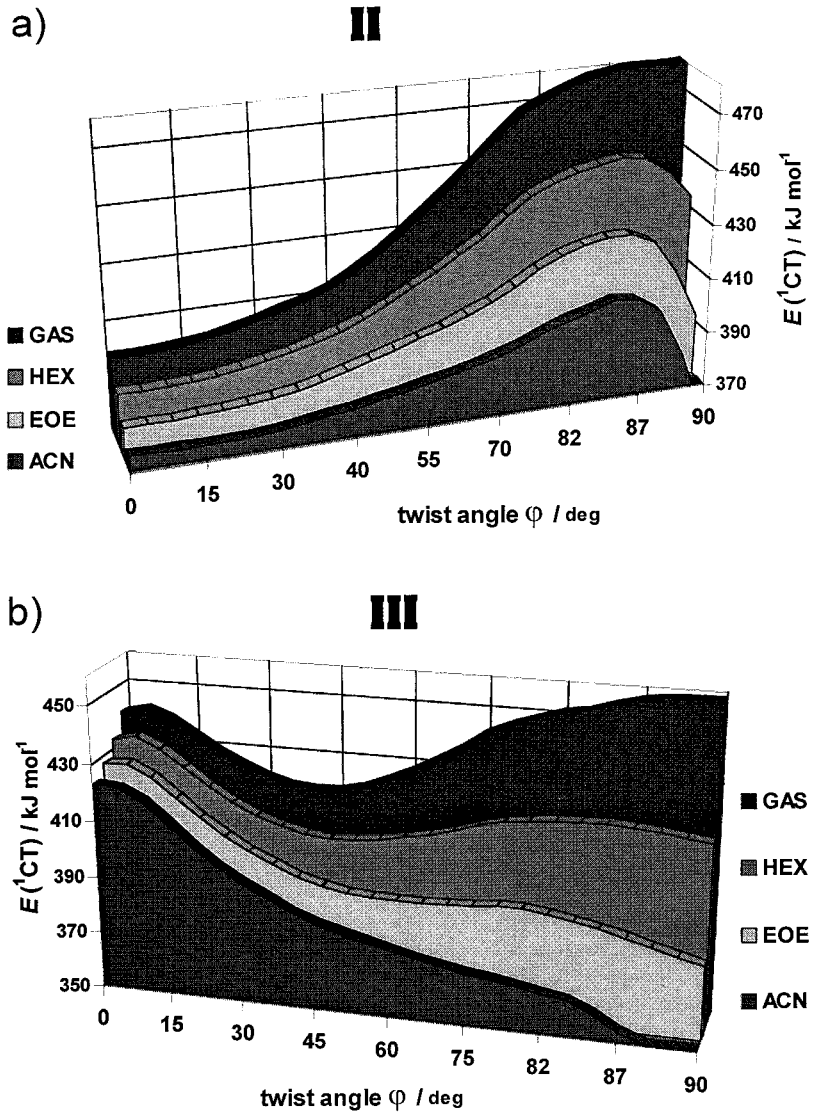

Figure 9. ^{1}CT twist potentials of (a) **II** and (b) **III** in solvents of different polarity as obtained by eq 4.

TABLE 5: Data from S_0 Twist Potentials[a]

	φ_{eq}	$E_i^{\#}(\varphi = 0°)$	$E_i^{\#}(\varphi = 90°)$	$\langle\varphi_\eta\rangle$
II	39°	5.2 kJ mol^{-1}	7.7 kJ mol^{-1}	34.5°
III	78°	66.3 kJ mol^{-1}	0.5 kJ mol^{-1}	72°

[a] Obtained by AM1/gas phase/298 K.

0) but high barriers ($E_i^{\#}(90°) > 30$ kJ) toward more twisted rotamers, whereas (b) **III** can populate two rotamer minima, the population of which is modulated by their solvent polarity-dependent energy difference and activation barrier ($E_i^{\#}(90°) = 0-40$ kJ). In nonpolar solvents such as HEX, only the more planar rotamer distribution is populated, which is experimentally observed as a more emissive species **CT**, and in highly polar solvents such as ACN, only the more twisted distribution **CTR** is observed with smaller emission rates k_f. In medium polar solvents such as EOE, a primary relaxation to the **CT** distribution with weak solvent stabilization can be assumed, followed by an equilibration between both rotamer distributions **CT** and **CTR**.

The above discussion can be further refined by a correlation of the experimental with the calculated reduced radiative rates, because they are monotonically decreasing with φ. If we employ the calculated $k_f/\nu^3(\varphi)$ curves of **II** and **III** in Figure 7c and 8c directly as calibration curves, ground and excited-state mean twist angles $\langle\varphi_{kf}(S_0)\rangle$ and $\langle\varphi_{kf}(S_1)\rangle$ can be approximated from the experimental Strickler−Berg rates $k_f^{SB}/\nu_f^3 n^3$ and fluorescence rates $k_f/\nu_f^3 n^3$ (Tables 3 and 4), respectively. The resulting ground and excited-state twist angles $\langle\varphi_{kf}(S_0)\rangle$ and $\langle\varphi_{kf}(S_1)\rangle$ of **II** and **III** are collected in Table 6. In agreement with the gas-phase AM1 optimizations, the obtained ground-state angles $\langle\varphi_{kf}(S_0)\rangle$ for **II** and **III** are around 40° and 80°, respectively. As expected, the radiative rates of **II** are consistent with a fully planar excited-state geometry in all solvents. In contrast, the S_1 conformation of **III** obtained is 20° more planar in HEX and 5° more twisted in ACN, as compared to the average S_0 conformation. For **III** in EOE, $\langle\varphi_{kf}(S_1)\rangle$ is intermediate between that of HEX and ACN. In light of the time-resolved experiments presented in Figures 4 and 5, this is understandable by an equilibrium between two rotamer distributions, one associated with more planar twist angles than $\langle\varphi(S_0)\rangle$ assignable to the precursor species **CT** and the other connected with more twisted angles than $\langle\varphi(S_0)\rangle$ assignable to the more relaxed successor species **CTR**.

4. Conclusions

This study provides a comprehensive survey of the fluorescence and photophysical behavior of the differently twisted donor−acceptor biphenyls **I**−**III** and related biphenyls. It

TABLE 6: S_1 Twist Angles and Energy Barriers As Derived from CNDO/S Calculations Using Eqs 2−4 (see Figure 9)

	$\varphi_{eq}(^1CT)^a$	$E_i^{\#}$ ($\varphi \rightarrow 0°$)^b	$E_i^{\#}$ ($\varphi \rightarrow 90°$)^b	$\langle\varphi_{kf}(S_0)\rangle^c$	$\langle\varphi_{kf}(S_1)\rangle^c$
			II		
GAS	0°	0 kJ	84 kJ		
HEX	0°(+ 90°)	0 kJ	61 kJ	49	0
EOE	0°(+ 90°)	0 kJ	45 kJ	40	0
ACN	5°(+ 90°)	0.5 kJ	31 kJ	35	0
			III		
GAS	40°	24 kJ	41 kJ		
HEX	45° (+ 90°)	31 kJ	14 kJ	82	64
EOE	60° (+ 90°)	40 kJ	2 kJ	82	78
ACN	90°	79 kJ	0 kJ	82	85

[a] Equilibrium twist angles of ^1CT potentials shown in Figure 9. [b] Intrinsic energy barrier for intramolecular rotation from the more planar minimum to the geometry with $\varphi = 0°$ and $\varphi = 90°$, respectively. [c] Mean angles obtained by a direct correlation of the experimental Strickler−Berg ($k_f^{SB}/n^3\nu_f^3$) and fluorescence ($k_f/n^3\nu_f^3$) rates with the calculation results in Figures 7c and 8c.

provides the desired conclusions on the electronic and conformational structure in the ground-state S_0 and the first excited singlet state S_1 reached after photoinduced intramolecular charge transfer.

The three problems complicating the photophysics of other known donor−acceptor biphenyls, as mentioned in the introductory section, can be excluded as follows.

Category 1 (S_1 State of Mixed ^1L_b- and ^1L_a-Type). The electronic nature of S_1 in **I**−**III** observed in the fluorescence can definitely be assigned to a pure ^1L_a-type $^1CT(2^1A)$ state (except for a small deviation of **I** in *n*-hexane where ^1L_b mixing is also important) transferring charge from the HOMO(D) to the LUMO(A) orbital across the interannular bond. The three main cornerstones for this assignment are (i) the large radiative rates ($k_f > 0.3$ ns^{-1} except for **III** in polar solvents), (ii) a degree of fluorescence polarization close to 0.5 ($p = 0.44-0.48$), and (iii) the comparison with CNDO/S calculated fluorescence energies, dipole moments, and radiative rates, which is consistent only with $^1CT(2^1A)$.

Category 2 (Strongly Polarity-Dependent Nonradiative Rates). The influence of the (bulk) solvent polarity on the nonradiative rates k_{nr} of **I**−**III** is weak and can be explained. In polar and aprotic solvents, k_{nr} remains constant at 0.1 ns^{-1} for all compounds studied. The higher rates in HEX ($\Delta k_{nr} =$ 0.2, 0.15, and 0.45 ns^{-1} for **I**−**III**) are understandable by an additional ISC channel, effective only in nonpolar solvents by a possible S_1-T_n level reversal. Thus, no strongly nonradiative channel due to intramolecular relaxations complicates the photophysics of **I**−**III**.

Category 3 (Specific Solvent Interactions in S_0 and S_1). Specific solvent interactions are weak or even absent in **I** and **II** and found only for **III** in EtOH by an enhancement of k_{nr} ($\Delta k_{nr} = 0.56$ ns^{-1}). Because the spectral and radiative properties of **III** are rather identical in EtOH and equipolar ACN, the nonradiative channel is not induced by polarity but by hydrogen bonding in S_1 only and can therefore be avoided, if only aprotic solvents are used.

Hence, the knowledge of the electronic nature and photophysics renders the donor−acceptor biphenyls **I**−**III** as excellent model compounds to investigate conformational changes with respect to the interannular twist angle φ in S_0 and S_1 associated with photoinduced charge transfer. The similar radiative rates k_f, excited-state dipole moments μ_e, and other fluorescence properties of **I** and **II** connected with a difference in their Strickler−Berg rates k_f^{SB} (k_f^{SB}(**I**) > k_f^{SB}(**II**) but k_f(**I**) = k_f(**II**)) show that the flexible compound **II** relaxes to a planar geometry after photoexcitation. In contrast, the higher nonradiative rates k_{nr} in *n*-hexane, larger excited-state dipole moments μ_e, and smaller radiative rates k_f and k_f^{SB} of **III** confirm the twisted structure of this sterically hindered derivative in S_0 and S_1. In contrast to **I** and **II**, the energy-corrected rates $k_f/\nu_f^3n^3$ of **III** decline with increasing polarity. The latter behavior can be explained with a solvent polarity-independent mean twist angle $\langle\varphi\rangle$ in S_0, whereas in S_1, the rotamer distribution is more planar in nonpolar solvents and more twisted in polar solvents as compared to S_0. The strongly twisted conformation in polar solvents leads to a biradicaloid electronic structure associated with electron localization on the benzonitrile acceptor unit. Therefore, the dynamic fluorescence quenching observed only for **III** in the protic solvent ethanol, which is interpreted by protic interaction of ethanol with the negatively charged benzonitrile unit, can be taken as further evidence of the highly twisted structure of **III** in polar solvents.

In the solvent of intermediate polarity, diethyl ether, the fluorescence decay is biexponential only for **III**. Together with the strong temperature dependence of the lifetimes and the spectral dependence of their amplitudes, this indicates the coexistence of two excited-state rotamer distributions. One of them is more planar (**CT**) and the other one more twisted (**CTR**) than the original distribution in the ground state. At room temperature, both rotamer distributions are in a fast equilibrium. The rise times observed at low temperature reveal a photoreaction with **CT** as precursor and the more relaxed **CTR** as successor species. The primary relaxation from the Franck−Condon geometry to the more planar geometry of the **CT** species, which takes place in all biphenyls during the solvation process, is not observed here because it is either too fast or the emission properties of the more planar rotamers are too similar to be detected by the time-resolved experiments.[77] The quantum chemical calculations in combination with the Onsager model support the experimental conclusions regarding the barrierless excited-state planarization of **II** in all solvents and of **III** in nonpolar solvents (**CT**), the occurrence of a double minimum potential for **III** in EOE (**CT** and **CTR**), and the preference of highly twisted conformers in more polar solvents (**CTR**).

In general, the results of these bichromophoric model molecules show that the introduction of strong Coulombic interactions (here by photoinduced charge transfer) connected with a different interplay of solvent and mesomeric stabilization not only determines the conformational structure but also can lead to an equilibrium of conformers with different π-conjugation.

References and Notes

(1) Grabowski, Z. R.; Rotkiewicz, K.; Siemiarczuk, A.; Cowley, D. J.; Baumann, W. *Nouv. J. Chim.* **1979**, *3*, 443.
(2) Rettig, W. *Angew. Chem., Int. Ed. Engl.* **1986**, *25*, 971.
(3) Zachariasse, K. *Pure Appl. Chem.* **1993**, *65*, 1745.
(4) Visser, R. J.; Cyril, A. G.; Varma, G. O. *J. Chem. Soc., Faraday Trans 2* **1980**, *76*, 453.
(5) Sobolewski, A. L.; Domcke, W. *Chem. Phys. Lett.* **1996**, *259*, 119.
(6) (a) Berlman, I. B.; Steingraber, O. J. *J. Chem. Phys.* **1965**, *43*, 2140. (b) Berlman, I. B. *J. Chem. Phys.* **1970**, *52*, 5616.
(7) Hohlneicher, G.; Dörr, F.; Mika, N.; Schneider, S. *Ber. Bunsen-Ges. Physik. Chem.* **1968**, *72*, 1144.
(8) Momicchioli, F.; Bruni, M. C.; Baraldi, I. *J. Phys. Chem.* **1972**, *76*, 3983 and references therein.
(9) (a) Dick, B.; Hohlneicher, G. *Chem. Phys.* **1985**, *94*, 131. (b) Rubio, M.; Merchán, M.; Ortí, E.; Roos, B. O. *Chem. Phys. Lett.* **1995**, *234*, 373. (b) Swiderek, P.; Michaud, M.; Hohlneicher, G.; Sanche, L. *Chem. Phys. Lett.* **1991**, *187(6)*, 583.
(10) (a) Kurland, R.; Wise, W. B. *J. Am. Chem. Soc.* **1964**, *86*, 1877. (b) Eaton, V. J.; Steele, D. *J. Chem. Soc., Faraday Trans. 2* **1973**, *69*, 1601.

(c) Le Gall, Suzuki, H. *Chem. Phys. Lett.* **1977**, *46*, 467. (d) Uchimura, H.; Tajiri, A.; Hatano, M. *Bull. Chem. Soc. Jpn.* **1981**, *54*, 3279; *Chem. Phys. Lett.* **1975**, *34*, 34. (e) d'Amibale, A.; Lunazzi, L.; Boicelli, A. C.; Macciantell, D. *J. Chem. Soc., Perkins Trans. 2* **1973**, *69*, 1396. (f) Lim, E.; Li, Y. H. *J. Chem. Phys.* **1970**, *52*, 6416. (g) Barrett, R. M.; Steele, D. *J. Mol. Struct.* **1972**, *11*, 105.

(11) Takei, Y.; Yamaguchi, T.; Osamura, Y.; Fuke, K.; Kaya, K. *J. Phys. Chem.* **1988**, *92*, 577.

(12) Butler, R. M., Lynn, M. A., Gustafson, T. L. *J. Phys. Chem.* **1993**, *97*, 2609.

(13) Swiatkowski, G.; Menzel, R.; Rapp, W. *J. Lumin.* **1987**, *37*, 183.

(14) (a) Lahmani, F.; Breheret, E., Zehnacker-Rentien, A.; Amatore, C.; Jutand, A. *J. Photochem. Photobiol., A* **1993**, *70*, 39. (b) Lahmani, F.; Breheret, E., Benoist d'Azy, O.; Zehnacker-Rentien, A; Delouis, J. F. *J. Photochem. Photobiol., A* **1995**, *89*, 191.

(15) (a) Klock, A. M.; Rettig, W. *Pol. J. Chem.* **1993**, *67*, 1375. (b) Maus, M.; Rettig, W.; Lapouyade, R. *J. Inf. Rec. Mater.* **1996**, *22*, 451. (c) Rettig, W.; Maus, M. *Ber. Bunsen-Ges. Phys. Chem.* **1996**, *100*, 2091.

(16) Herbich, J.; Waluk, J. *Chem. Phys.* **1994**, *188*, 247.

(17) (a) Ephardt, H.; Fromherz, P. *J. Phys. Chem.* **1991**, *95*, 6792. (b) Fromherz, P., Heilemann, A. *J. Phys. Chem.* **1992**, *96*, 6864. (c) Röcker, C., Heilemann A.; Fromherz, P. *J. Phys. Chem.* **1996**, *100*, 12172.

(18) Chou, P. T.; Chang, C. P.; Clements, J. H.; Meng-Shin, K. *J. Fluoresc.* **1995**, *5*, 369.

(19) David, C.; Baeyens-Volant, D. *Mol. Cryst. Liq. Cryst.* **1980**, *59*, 181.

(20) Lippert, E. *Ber. Bunsen-Ges. Phys. Chem. (Z. Elektrochem.)* **1957**, *61*, 962.

(21) Zhu, Y.; Schuster, G. B. *J. Am. Chem. Soc.* **1990**, *112*, 8583.

(22) Foley, M. J.; Singer, L. A. *J. Phys. Chem.* **1994**, *98*, 6430.

(23) Cowley, D. J.; O'Kane, E.; Todd, R. S. J. *J. Chem. Soc., Perkin Trans. 2* **1991**, 1495.

(24) Lequan, M.; Lequan, R. M.; Ching, K. C. *J. Mater. Chem.* **1991**, *1*, 997.

(25) (a) Yoon, M.; Cho, D. W.; Lee, J. Y. *Bull. Korean Chem. Soc.* **1992**, *13*, 613. (b) Kang, S. G.; Ahn, K. D.; Cho, D. W.; Yoon, M. *Bull. Korean Chem. Soc.* **1995**, *16*, 972. (c) Cho, D. W.; Kim, Y. H.; Kang, S. G.; Yoon, M. *J. Phys. Chem.* **1994**, *98*, 558. (d) Cho, D. W.; Kim, Y. H.; Kang, S. G.; Yoon, M.; Kim, D. *J. Chem. Soc. Faraday Trans.* **1996**, *92*, 29.

(26) Maus, M.; Rettig, W. *Chem. Phys.* **1997**, *218*, 151.

(27) Suzuki, H. *Electronic Absorption Spectra and Geometry of Organic Molecules*; Academic Press: New York, 1967.

(28) (a) Longuet-Higgins, H. C.; Murrell, J. N. *Proc. Phys. Soc. A* **1955**, *68*, 601. (b) Godfrey M.; Murrell, J. N. *Proc. R. Soc. A* **1966**, 278, 60.

(29) In the present notation, a distinction is made between ^{1}ET and ^{1}CT. ^{1}ET represents the case for a complete transfer of one electron from D to A, whereas ^{1}CT denotes a state with partial electron transfer resulting from mixed locally excited and ^{1}ET character.

(30) Maus, M. Ph.D. Thesis, *Photoinduced Intramolecular Charge Transfer in Donor−Acceptor Biaryls and Resulting Applicational Aspects Regarding Fluorescent Probes and Solar Energy Conversion*, http:/www.dissertation.com/library/1120303a.htm, 1998.

(31) Maus, M.; Rettig, W.; Jonusauskas, G.; Lapouyade, R.; Rullière, C. *J. Phys. Chem.* **1998**, *102*, 7393.

(32) Gribble, G. W.; Nutaitis, C. F. *Synthesis* **1987**, 709.

(33) Ellis, G. P.; Romney-Alexander, T. M. *Chem. Rev.* **1987**, *87*, 779.

(34) Fox, G. J.; Hallas, G.; Hepworth, J. D.; Paskins, K. N. *Org. Synth.* **1976**, *55*, 20.

(35) McNamara, J. M.; Gleason, W. B. *J. Org. Chem.* **1976**, *41*, 1071.

(36) Amatore, C.; Jutand, A.; Negri, S.; Fauvarque, J.-F. *J. Organomet. Chem.* **1990**, *390*, 389.

(37) Parker, C. A. *Photoluminescence of Solutions*; Elsevier: Amsterdam, 1968.

(38) Melhuish, W. H. *J. Phys. Chem.* **1961**, *65*, 229.

(39) Globals Unlimited, commercially available from the Laboratory of Fluorescence Dynamics at the University of Illinois, 1992.

(40) O'Connor, D. V.; Phillips, D. *Time-correlated Single Photon Counting*; Academic Press: London, 1984.

(41) Del Bene, J.; Jaffe, H. H. *J. Chem. Phys.* **1968**, *48*, 1807; **1968**, *48*, 4050; **1968**, *49*, 1221; **1969**, *50*, 1126.

(42) AMPAC 5.0; Semichem, 7128 Summit, Shawnee, KS 66216, 1994. Dewar, M. J. S.; Zoebisch, E. G.; Healy, E. F.; Stewart, J. P. *J. Am. Chem. Soc.* **1985**, 107, 3902.

(43) Onsager, L. *J. Am. Chem. Soc.* **1936**, *58*, 1486.

(44) Zerner, M. C.; Karelson, M. M. *J. Phys. Chem.* **1992**, *96*, 6949.

(45) Commercially available from Serena Software, Box 3076, Bloomington, IN 47402−3076.

(46) Böttcher, C. J. F. *Theory of Electronic Polarisation*; Elsevier: Amsterdam, 1973.

(47) Marcus, R. A. *J. Phys. Chem.* **1989**, *93*, 3078.

(48) Lippert, E. *Z. Naturforsch.* **1955**, *10a*, 541.

(49) Mataga, N.; Kaifu, Y.; Koizumi, M. *Bull. Chem. Soc. Jpn.* **1956**, *29*, 465.

(50) McRae, E. G. *J. Phys. Chem.* **1957**, *61*, 562.

(51) Bilot, L.; Kawski, A. *Z. Naturforsch.* **1962**, *17a*, 621.

(52) Létard, J. F.; Lapouyade, R.; Rettig, W. *J. Am. Chem. Soc.* **1993**, *115*, 2441.

(53) Riddick, J. A.; Bunger, W. B.; Sakano, T. K. *Organic Solvents*; John Wiley & Sons: New York, 1986.

(54) Klock, A. M.; Rettig, W.; Hofkens, J.; van Damme, M.; De Schryver, F. C. *J. Photochem. Photobiol., A* **1995**, *85*, 11.

(55) Van Damme, M.; Hofkens, J.; De Schryver, F. C. *Tetrahedron* **1989**, *45*, 4693.

(56) Grabowski, Z. R.; Rotkiewicz, K.; Siemiarczuk, A. *J. Lumin.* **1979**, *18/19*, 420.

(57) Flom, S. R., Nagarajan, V.; Barbara, P. F. *J. Phys. Chem.* **1986**, *90*, 2085.

(58) Ma, J.; Dutt, G. B.; Waldeck, D. H.; Zimmt, M. B. *J. Am. Chem. Soc.* **1994**, *116*, 10619.

(59) Strehmel, B.; Seifert, H.; Rettig, W. *J. Phys. Chem.* **1997**, *101*, 2232.

(60) Possible ^1L_b contribution of the H band to $\int \epsilon d\nu_a$ can be neglected because almost all of its intensity is borrowed from ^{1}CT. However, the absorption spectrum $\epsilon(\nu_a)$ of the CT band has been corrected for the contributions of the A and B bands by subtraction of these bands fitted to Gaussian functions.

(61) Birks, J. B. *Photophysics of Aromatic Molecules*; Wiley-Interscience: New York, 1970.

(62) Förster, T. *Fluoreszenz organischer Verbindungen*; Vanderhoeck and Ruprecht: Göttingen, 1951.

(63) Schütz, M.; Schmidt, R. *J. Phys. Chem.* **1996**, *100*, 2012.

(64) Fujii, T.; Suzuki, S.; Komatsu, S. *Chem. Phys. Lett.* **1978**, *57*, 175.

(65) Ikeda, N.; Miyasaka, H.; Okada, T.; Mataga, N. *J. Am. Chem. Soc.* **1983**, *105*, 5206.

(66) Blias, J.; Gauthier, M. *Opt. Spectrosc.* **1978**, *9*, 529.

(67) López Arbeloa, T.; López Arbeloa, F.; López Arbeloa, I. *J. Lumin.* **1996**, *68*, 149. López Arbeloa, T.; López Arbeloa, F.; Hernández Bartolomé, P.; López Arbeloa, I. *Chem. Phys.* **1992**, *160*, 123.

(68) Kakitani, T.; Mataga, N. *J. Phys. Chem.* **1986**, *90*, 993; **1987**, *91*, 6277.

(69) Strehmel, B.; Rettig, W. *J. Biomed. Opt.* **1996**, *1*, 98.

(70) Strickler, S. J.; Berg, R. A. *J. Chem. Phys.* **1962**, *37*, 814.

(71) At temperatures below −90°, an additional minor time component with small amplitudes only in the very blue wing of the fluorescence band has been used for the global analysis of the exponential fits of all three compounds. Because **I** also needs this time constant, it is not related to twisting. This very short component can be attributed to solvent friction effects, the relaxation times of which fall into the time resolution of the experimental setup under highly viscous conditions at low temperatures.

(72) Because a plot of the amplitude ratio α_2/α_1 reaches a plateau in the blue edge of the fluorescence spectrum, the CTR deactivation rate constant Y (eq 12d) can be derived in the blue spectral region from $\alpha_2/\alpha_1 = (\tau_2^{-1} - Y)/(Y - \tau_1^{-1})$. It turns out that Y is close to τ_2^{-1}, in particular for the temperatures below 223 K. This indeed indicates that the adiabatic photoreaction is dominantly in the irreversible region.

(73) Rettig, W.; Fritz, R.; Braun, D. *J. Phys. Chem.* **1997**, *A101*, 6830.

(74) Zachariasse, K.; Grobys, M.; von der Haar, T.; Hebecker, A.; Il'ichev, Yu. V.; Jiang, Y.-B.; Morawski, O.; Kühnle, W. *J. Photochem. Photobiol., A* **1996**, *102*, 59.

(75) To account for the $n^3\nu_f^3$ dependence and the k_{nr} difference, the intrinsic lifetimes in EOE can be calculated by $\tau_0(\mathrm{CT}) = 1/(k_{nr}(\mathrm{EOE}) + k_f(\mathrm{HEX})(\nu_f(\mathrm{EOE})^3 n_f(\mathrm{EOE})^3/\nu_f(\mathrm{HEX})^3 n_f(\mathrm{HEX})^3))$ and $\tau_0(\mathrm{CTR}) = 1/(k_{nr}(\mathrm{EOE}) + k_f(\mathrm{HEX})(\nu_f(\mathrm{EOE})^3 n_f(\mathrm{EOE})^3/\nu_f(\mathrm{ACN})^3 n_f(\mathrm{ACN})^3))$ In addition, if we suppose the radiative rates as temperature-independent, the nonradiative rates in EOE at 160 K can be obtained from $k_{nr}(160\ \mathrm{K}) = k_{nr}(298\ \mathrm{K}) - \tau_0(298\ \mathrm{K})^{-1} + \tau_0(160\ \mathrm{K})^{-1}$. For the **CT** species $k_{nr}(160\ \mathrm{K}) = 5 \times 10^7\ \mathrm{s}^{-1}$, and for the **CTR** species $k_{nr}(160\ \mathrm{K}) = 3 \times 10^7\ \mathrm{s}^{-1}$. These values are rather similar to the room-temperature value of $k_{nr}(298\ \mathrm{K}) = 10 \times 10^7\ \mathrm{s}^{-1}$, and the corresponding activation barrier is then less than RT. The neglection of $k_{nr}(T)$ in eq 13 is therefore justified (cf. τ_1^{-1} (298 K) − τ_1^{-1} (160 K) = $500 \times 10^7 \mathrm{s}^{-1}$).

(76) The dimethylamino group is calculated to be coplanar with the linked phenyl unit in S_0, S_1, and S_2. A negligible deviation from C_2 symmetry is found only for S_0, where the pyramidalization angle is not exactly planar.

(77) In a recent paper (Verbouwe, W.; Viaene, L.; Auweraer, V.d.; DeSchryver, F. C.; Masuhara, H.; Pansu, R.; Faure, J. *J. Phys. Chem. A* **1997**, *101*, 8157.) donor-substituted biphenyls were also found to relax to a planar geometry, despite monoexponential emission decays within a time-resolution of 20 ps.